In-situ monazite geochronological constraints on the timing of vein formation and gold mineralization in the Klondike gold district, western Yukon

*Brodie A. Stroh**
Cameco Corporation
Mineral Deposit Research Unit, University of British Columbia

Tyler K. Ambrose
Yukon Geological Survey
Mineral Deposit Research Unit, University of British Columbia

Murray M. Allan
Teck Resources Limited
Mineral Deposit Research Unit, University of British Columbia

Matthijs A. Smit
Department of Earth, Ocean & Atmospheric Sciences, University of British Columbia

Stroh, B.A., Ambrose, T.K., Allan, M.A. and Smit, M.A., 2026. In-situ monazite geochronological constraints on the timing of vein formation and gold mineralization in the Klondike gold district, western Yukon. *In*: Yukon Exploration and Geology 2025, A. Stuart, L.H. Weston and S.K. Schultz (eds.), Yukon Geological Survey, Government of Yukon, p. 239–266, plus digital appendices.

Abstract

Orogenic gold deposits form some of the world's largest gold sources; however, the timing of mineralization is commonly difficult to constrain due to a lack of suitable geochronometers. Most studies rely on $^{40}Ar/^{39}Ar$ dating of mica, which is susceptible to thermal resetting and can be difficult to genetically link to gold deposition. Uranium-thorium-lead (U-Th-Pb) dating of monazite, which crystallizes in metamorphic and in some cases hydrothermal settings, provides an alternative that is not commonly applied to mineral deposits. Approximately 20 Moz of placer gold mined in the Klondike gold district was derived from orogenic, gold-bearing quartz veins of unknown age. In this study, we integrate monazite dates and geochemical analyses with petrographic observations to constrain the age of metamorphic and hydrothermal monazite growth. Our results reveal metamorphic monazite growth between 190 and 150 Ma, overlapping with burial and subsequent regional exhumation of the Yukon-Tanana terrane. Metamorphic monazite occurs with other metamorphic minerals regardless of proximity to veins, and has variable ThO_2 concentrations that depend on the composition of the host rock and metamorphic grade. Hydrothermal monazite dates ranging from 180 to 120 Ma record the duration of vein formation and bracket the timing of gold mineralization. Hydrothermal monazite occurs in, or adjacent to, veins with other hydrothermal minerals and has distinctly low ThO_2 concentrations (<2 wt%). Our findings underpin the complexity and longevity of vein formation in orogenic gold deposits, and demonstrate the utility of monazite in obtaining time-resolved information on this economically relevant process.

* brodie.stroh20@gmail.com

Plain language summary

Most gold in the Klondike goldfields occurs as loose grains and nuggets in river gravel—known as placer gold—deposited over the past several million years. The gold grains likely came from nearby quartz veins in bedrock. Although the age of the placer deposits is fairly well understood, the timing of the quartz veins and especially the gold within them is poorly constrained. To determine the age of the quartz veins and gold mineralization we combined fieldwork and sample collection with laboratory analyses. We focused on monazite, a mineral whose chemical composition can be used to date geological processes. Our results indicate that the rocks exposed in the Klondike region were metamorphosed (i.e., buried, deformed and heated) between approximately 190 and 150 million years ago, and that the veins formed from 180 to 120 million years ago. Our work highlights the utility of monazite and provides insight into the timescale of vein formation and gold mineralization in the Klondike.

Introduction

Orogenic gold deposits typically form at convergent plate margins along structures that act as conduits for hydrothermal fluids generated during metamorphism (e.g., Groves et al., 1998; Bierlein and Crowe, 2000; Goldfarb et al., 2001; Groves et al., 2003; Goldfarb et al., 2005; Goldfarb and Groves, 2015; Mortensen et al., 2023). In contrast to most other gold-bearing deposit types, orogenic gold deposits are not genetically linked with magmatism (Goldfarb and Pitcairn, 2022). Instead, the mineralizing fluid is inferred to be produced by devolatilization reactions during regional metamorphism at pressures and temperatures corresponding to the greenschist-amphibolite transition zone (e.g., Henley et al., 1976; Goldfarb et al., 1991; Stuwe, 1998; Pitcairn et al., 2006). The fluid is channeled through permeable structures and driven upwards before precipitating gold-bearing quartz veins at 3–15 km depth (Groves et al., 1998; Goldfarb and Groves, 2015; White et al., 2015). Orogenic gold deposits form some of Earth's largest gold deposits (e.g., Ashanti, Ghana, 3169 t at 2–7 g/t Au; Golden Mile, Australia, 2079 t at 2 g/t Au; Frimmel, 2008). Still, several components of their generation are highly debated (e.g., Goldfarb and Groves, 2015), including the source of the gold, controls on deposition, and the absolute timing of mineralization.

The formation of orogenic gold deposits typically occurs during or after peak metamorphism of the host rocks (Groves et al., 1998). The timing of orogenic gold formation can be constrained by various methods: $^{40}Ar/^{39}Ar$ dating of muscovite, sericite and biotite (e.g., Bierlein et al., 2001; Mortensen et al., 2010); $^{187}Re/^{187}Os$ dating of arsenopyrite and molybdenite (e.g., Arne et al., 2001; Selby et al., 2002); and U-Pb dating of zircon, titanite and rutile (e.g., Kerrich and King, 1993; Lin and Corfu, 2002). However, determining the precise timing of mineralization is typically non-trivial; geochronometric minerals are often too small to analyze or may have been reset by later hydrothermal events. The latter applies particularly to white mica. Although this phase is common in quartz veins and is the most commonly used geochronometer, its low closure temperature (e.g., ~380°C for muscovite; Reiners and Brandon, 2006) means that it is vulnerable to resetting by later thermal events and fluids. Another issue is that chronometric minerals often lack a clear paragenetic relationship with gold, which leaves uncertainty as to whether the age data represent the timing of vein emplacement or specific vein phases that are associated with gold formation (e.g., Grimshaw, 2018).

Monazite and xenotime U-Th-Pb geochronology are less commonly applied techniques for dating orogenic gold mineralization. These approaches nevertheless have several advantages over $^{40}Ar/^{39}Ar$ white mica dating (e.g., Brown et al., 2002; Vielreicher et al., 2003; Salier et al., 2005; Sarma et al., 2008; Taylor et al., 2015). Monazite is less susceptible to thermal resetting due to its high closure temperature of >800°C (Cherniak et al., 2004), but can be modified by fluid-rock interaction, which can be exploited to date hydrothermal events (Williams et al., 2011). Monazite composition is indicative of petrological processes such as the growth or breakdown of other minerals during crystallization, thus enabling links between age data and mineral reactions (e.g., Pyle and Spear, 1999; Kylander-Clark et al., 2013). These features make monazite very useful in obtaining temporal constraints on geological events and processes. Though such studies have mostly focused on metamorphic rocks, the concepts can also be applied to ore deposits. For example, Schandl and Gorton (2004) used ThO_2 concentrations to distinguish between hydrothermal and igneous monazite, and Taylor et al. (2015) used

europium (Eu) anomalies to identify hydrothermal monazite in the Grass Valley orogenic gold district of California. Linking monazite growth or recrystallization to orogenic gold formation is the next frontier and requires establishing a paragenetic relationship with gold, particularly because monazite can grow through metamorphic or hydrothermal processes. In this study, we explore this for the Klondike gold district in the northwestern Canadian Cordillera.

The Klondike gold district hosts both orogenic gold occurrences and placer gold deposits. An estimated 20 Moz of placer gold were recovered from gold-bearing creeks in the Klondike from an area of ~1200 km^2 (Burke et al., 2005). Microchemical and grain shape analysis of placer grains indicates that the gold is sourced from orogenic quartz veins (e.g., Knight et al., 1999a,b; Mortensen et al., 2004, 2006; Crawford, 2007; Crawford et al., 2007; Chapman et al., 2010a,b, 2011). A regionally widespread, orogenic gold mineralization event in the Late Jurassic has been proposed for the Klondike, Sixtymile and White Gold metallogenic belts of western Yukon (Allan et al., 2013; Bailey, 2013); however, the timing of mineralization in the Klondike itself remains poorly constrained. Gold-bearing quartz veins in the Klondike have yielded $^{40}K/^{40}Ar$ and $^{40}Ar/^{39}Ar$ dates from 183 to 134 Ma (Hunt and Roddick, 1992; Breitsprecher and Mortensen, 2004; Joyce et al., 2015). The only direct age constraint for gold mineralization in the Klondike is an unpublished U-Pb date of 156 ± 8 Ma (Late Jurassic) from hydrothermal rutile in a gold-bearing quartz vein (Mortensen unpublished data, 2012, in Allan et al. 2013).

To constrain the timing of quartz vein emplacement and gold mineralization in the Klondike, we integrated field observations, petrography, whole-rock major and trace-element analysis, mineral major-element analysis, and monazite geochronology. We established a paragenetic framework for veins and alteration through petrographic analysis, quartz vein cathodoluminescence, and whole-rock composition. Our results provide a means to distinguish between metamorphic and hydrothermal monazite. Though we are unable to precisely date the timing of gold mineralization, our results constrain the timing of metamorphism and vein formation. The methods we establish can be applied to other orogenic gold deposits and metamorphic terranes in general.

Monazite growth mechanisms

Monazite is a light rare earth element (LREE) phosphate (PO_4) mineral and is a common accessory mineral in a wide variety of igneous, sedimentary, metamorphic and hydrothermal rocks (Overstreet, 1967). In orogenic gold settings, monazite can grow through both metamorphic and hydrothermal processes. Metamorphic monazite grows by the breakdown of other LREE- or phosphorus (P)-bearing minerals such as allanite, apatite and pre-existing monazite. It commonly forms in metamorphic rocks at amphibolite-facies conditions, but may also grow under greenschist-facies pressures and temperatures (Rasmussen et al., 2007; Williams et al., 2007; Allan et al., 2013; Grand'Homme, 2016). Intergranular fluids that facilitate metamorphic monazite growth through local dissolution and precipitation are typically locally generated and in thermodynamic equilibrium with the host rock. In contrast, hydrothermal monazite precipitates from externally derived hydrothermal fluid that has traveled through interconnected open spaces (i.e., flowed from metre to kilometre scales along permeable structures) and may be out of thermodynamic equilibrium with the host rock. Thus, hydrothermal monazite is only expected to form in and adjacent to veins (Fig. 1). Monazite can also grow by a mixture of local and external fluids, such as the growth of metamorphic monazite adjacent to a vein. Understanding the mechanism(s) by which monazite grows is essential when interpreting dates. To distinguish between metamorphic and hydrothermal monazite, we developed a framework based on petrographic associations, chemical zoning, and thorium (Th) and REE concentrations (Table 1 and Fig. 1).

Regional and local geology

The Klondike gold district is underlain by metaigneous and metasedimentary rocks of the northern Yukon-Tanana terrane (Fig. 2; Nelson et al., 2013). In the Yukon, the Yukon-Tanana terrane consists of three metamorphosed Devonian to Permian magmatic arc successions (Finlayson, Klinkit and Klondike assemblages) built upon metasedimentary rocks of the Neoproterozoic–Devonian Snowcap assemblage (Colpron et al., 2006).

The Klondike assemblage (commonly known as the Klondike schist; 269–253 Ma; Colpron et al., 2006) occurs throughout much of the district and is divided into five units by Mortensen et al. (2019): 1) a felsic package comprising quartz-muscovite-feldspar schist interpreted to be derived from a felsic volcanic or volcaniclastic rock; 2) a quartz-augen schist derived from a felsic quartz ± feldspar-phyric porphyry; 3) a mafic package comprising feldspar-chlorite-quartz ±

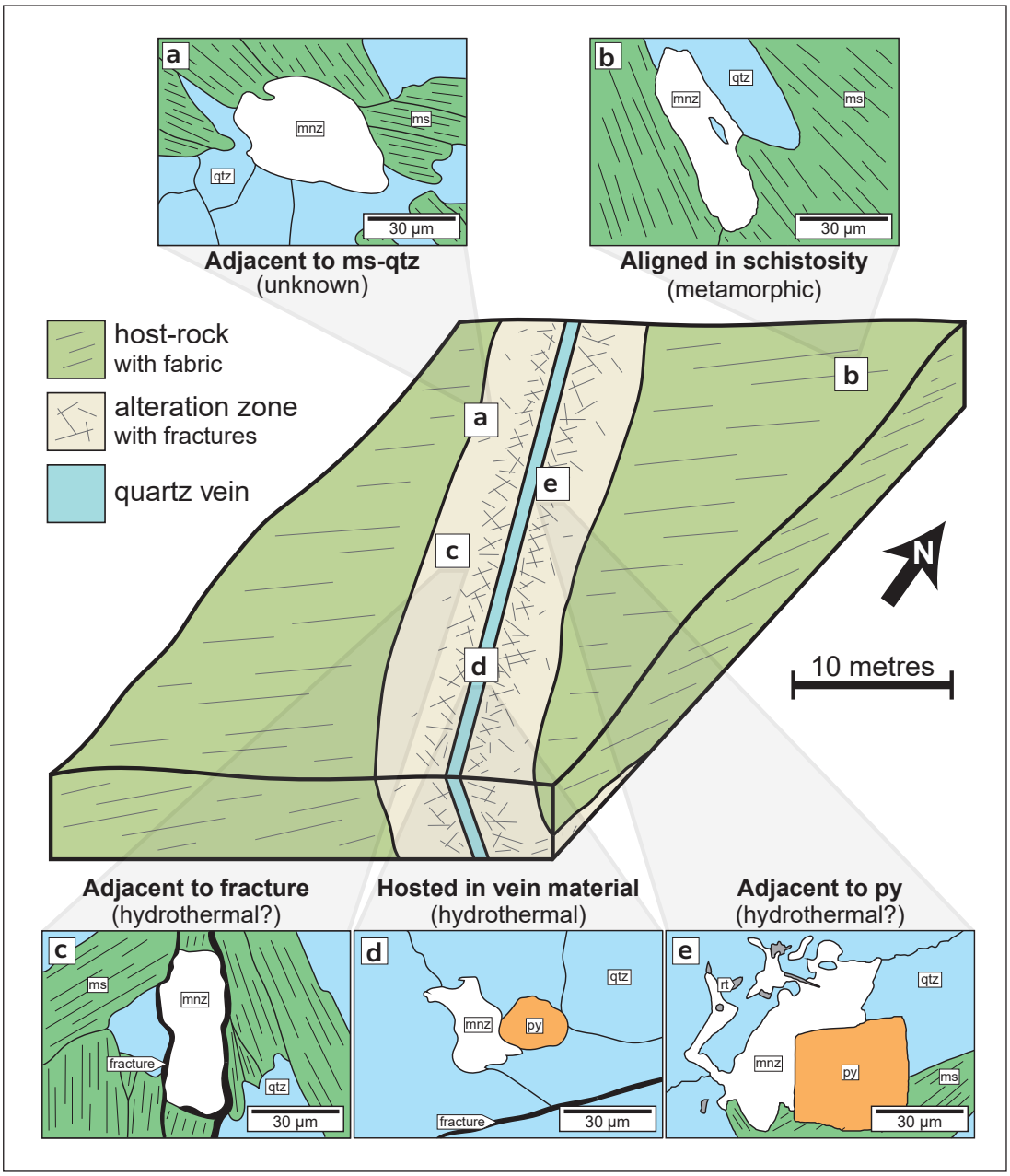

Figure 1. *Schematic diagram illustrating different petrographic contexts of monazite in orogenic gold settings (qtz – quartz; mnz – monazite; ms – muscovite; py – pyrite). The block diagram shows a quartz vein and alteration zone cutting through unaltered metamorphic rock. Schematics* **(a)–(e)** *each represent the expected monazite relationships for different geological settings and textures at each location. Next to each image are the petrographic associations in bold and interpretation in brackets. Only (b) and (d) can be confidently unambiguously interpreted because of their locations in the unaltered host rock and vein.*

epidote ± amphibole ± carbonate schist derived from intermediate or mafic volcanic or volcaniclastic rocks; 4) a metaclastic unit derived from quartz-rich clastic sedimentary rocks; and 5) an undifferentiated package that consists of intimately interlayered components of the felsic, mafic and metaclastic units. Most rocks in the Klondike assemblage are metavolcanic, though plutonic equivalents occur throughout the district (e.g., felsic metaporphyry and metagabbro of Mortensen, 1990).

Gold mineralization occurs in steeply to moderately dipping quartz-sulphide ± carbonate veins that cut the

Table 1. Indicators used to distinguish between different monazite growth mechanisms. The reliability of each indicator decreases towards the bottom. Mineral abbreviations: ab – albite; bt – biotite; fsp – feldspar; qtz – quartz.

Indicator	Igneous	Metamorphic	Hydrothermal	Reference(s)
Petrographic associations	• intergrown with igneous minerals and textures (e.g., qtz, fsp, bt)	• intergrown with metamorphic minerals and textures (e.g., bt)	• intergrown with hydrothermal minerals and textures (e.g., sulphides, oxides, micas, ab, qtz)	• Schandl and Gorton, 2004 • this study
ThO_2 concentration	• 3 to 13 wt% • lower in carbonatites	• 0 to >20 wt% • generally increases with metamorphic grade • dependent on protolith composition	• typically <2 wt%	• Schandl and Gorton, 2004 • Williams et al., 2007 • Cuney and Kyser, 2015 • Taylor et al., 2015 • Kohn and Malloy, 2004 • this study
REE geochemistry	• variable to significant europium (Eu) anomaly	• negative Eu anomaly (smaller after plagioclase breakdown)	• variable to no negative Eu anomaly	• Schandl and Gorton, 2004 • Williams et al., 2007 • Taylor et al., 2015
Other element concentrations	• high uranium (U)	• U and, to a lesser extent, thorium (Th) and yttrium (Y) increase with grade	• high U/Th	• Taylor et al., 2015 • Grand'Homme, 2016
Element zonation	• concentric • sector	• patchy • mottled • intergrowth-like • concentric • strongest Th zonation	• none • mottled • patchy	• Zhu and O'Nions, 1999 • Spear and Pyle, 2002 • Schandl and Gorton, 2004 • Williams et al., 2007 • Didier, 2013
Grain distribution	• sparse and homogeneous	• sparse and homogeneous	• commonly occurs in clusters	• Schandl and Gorton, 2004 • Williams et al., 2007 • this study
Grain size	• unknown	• <10 to >200 µm • increases with grade	• commonly <20 µm	• Schandl and Gorton, 2004 • Rasmussen et al., 2006

dominant foliation (Mortensen et al., 1992; Rushton et al., 1993). The veins are tabular to irregular, typically occur in anastomosing swarms with northeast or northwest trends, and are locally up to three metres wide (MacKenzie et al., 2008a). Texturally, they appear massive and only rarely display syntaxial growth textures typical of multiple crack-seal events (Allan et al., 2013). The veins consist almost entirely of milky white quartz (~98%) with minor pyrite and lesser carbonate, feldspar, muscovite, barite, scheelite, chalcopyrite, galena, sphalerite, rutile and sulfosalts (Hoymann and Friedrich, 1990). Gold typically occurs with pyrite along the vein margins and as free grains (Rushton et al., 1993). Hydrothermal alteration is relatively subtle and is expressed through assemblages comprising pyrite-sericite ± Fe-carbonate (e.g., mafic-hosted Mitchell-Sheba occurrences), kaolinite-silica (quartz-K-feldspar; e.g., metaporphyry-hosted Virgin occurrence), and minor silica (quartz)-pyrite (e.g., felsic-hosted Lone Star occurrence). Fluid inclusions in vein quartz exhibit low salinity (<6 wt% NaCl equivalent), heterogeneous CO_2 content, and reflect trapping conditions between 200 and 350°C and 300 to 2300 bar (Rushton et al., 1993). Rushton et al. (1993) interpreted the range in trapping conditions to reflect rapid exhumation during vein formation. All veins in the Klondike are broadly similar in terms of structural style, mineralogy, texture and fluid chemistry. It is therefore assumed that they

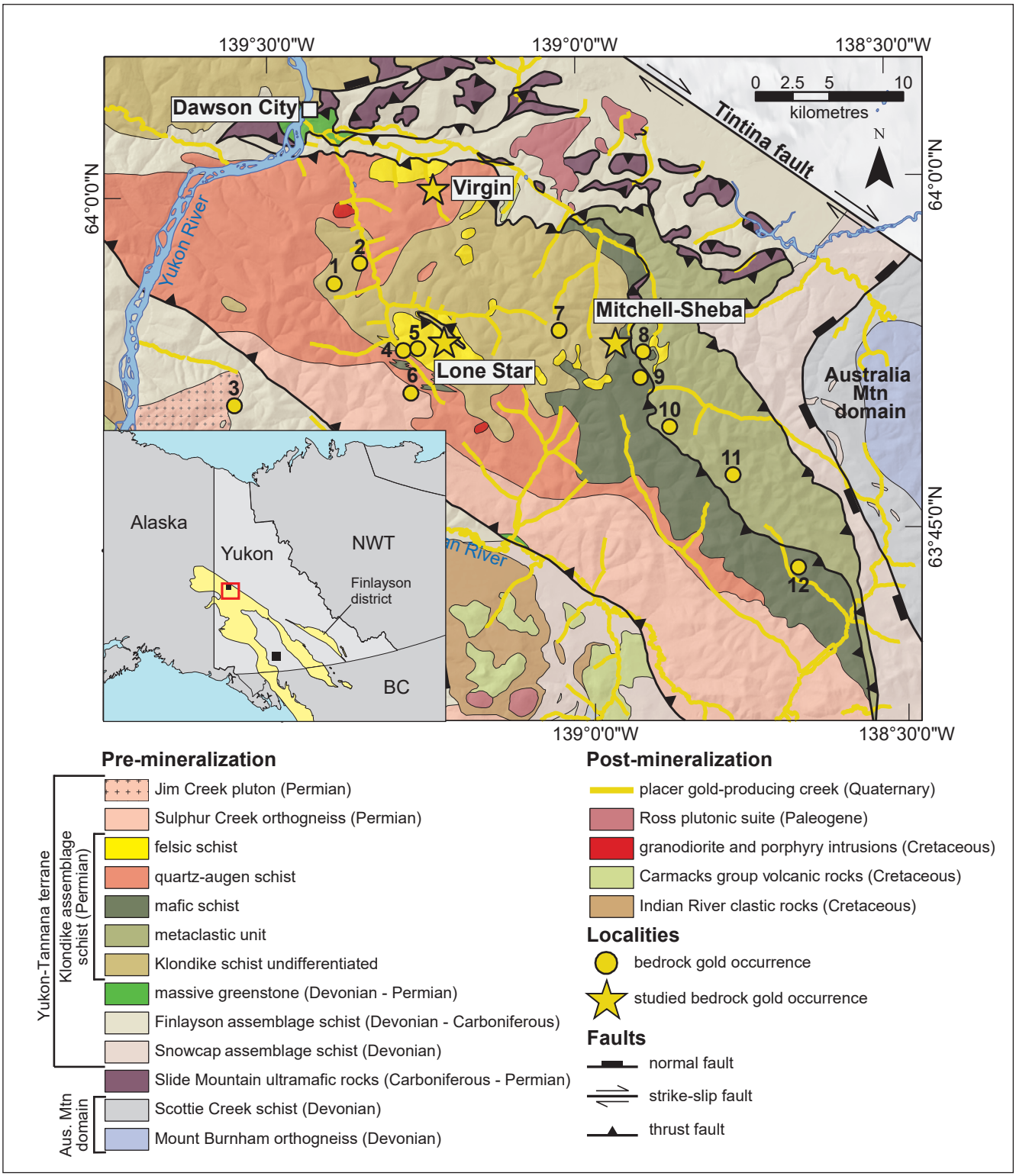

Figure 2. *Simplified geological map of the Klondike gold district (modified from Mortensen, 1996; Gordey and Ryan, 2005; Mortensen et al., 2019). Inset: Yukon-Tannana terrane is yellow; Whitehorse is the large black square; Dawson City is the small black square; map location is the red box. Studied localities are starred and labelled on the map. Other localities are labelled as numbered yellow dots: 1) Plinc; 2) Orofino; 3) IND; 4) Dysle; 5) Nugget; 6) Violet; 7) Boxcar; 8) MacKay; 9) Dome Lode/Hunker Dome; 10) Lloyd; 11) Gold Run; and 12) Aime/Payne.*

represent a single, albeit possibly protracted orogenic gold-forming event (Rushton et al., 1993; Mackenzie et al., 2008a; Allan et al., 2013).

In this study we investigated four bedrock gold occurrences: Virgin, Mitchell, Sheba and Lone Star. The Virgin gold occurrence (Yukon MINFILE 116B 007; Yukon Geological Survey, 2010) is hosted in a quartz-augen, quartz-albite-muscovite ± K-feldspar schist of the quartz-augen subunit (Mortensen, 1996; Mortensen et al., 2019). Quartz ± pyrite veins are associated with a kaolinite-quartz-K-feldspar-pyrite alteration halo. The Mitchell and Sheba gold occurrences (collectively known as Mitchell-Sheba; Yukon MINFILE 115O 068; Yukon Geological Survey, 2010) occur approximately 850 m apart along the same north-south trending vein system. The host rock at Mitchell-Sheba is an albite-chlorite-epidote-muscovite ± carbonate ± quartz ± amphibole schist of the mafic schist subunit (Mortensen, 1996; Mortensen et al., 2019). Quartz ± pyrite ± galena veins occur at Mitchell-Sheba with a muscovite-carbonate-pyrite alteration halo that is locally gold-bearing (Mortensen et al., 1992; Rushton et al., 1993; Chapman et al., 2010b). The Lone Star gold occurrence (Yukon MINFILE 115O 072; Yukon Geological Survey, 2010) is hosted in a quartz-muscovite-albite-chlorite schist of the felsic schist subunit (Mortensen, 1996; Mortensen et al., 2019). Quartz ± pyrite ± galena veins at Lone Star locally have a quartz-pyrite alteration halo. The Lone Star and Virgin occurrences are the only localities in the Klondike that have been mined for bedrock gold, albeit with negligible production (Allan et al., 2013). Modern exploration has focused in the Lone Star area, recently culminating in a 2022 NI-43-101 compliant resource of 469 Koz Au at 0.68 g/t Au (Indicated) and 112 Koz Au at 0.54 g/t Au (Inferred) by Klondike Gold Corporation between Lone Star and the newly discovered Stander zone (Jutras and Kenwood, 2022).

Methods

Below is a summary of our methodology that is described in full in Stroh (2019).

Sampling strategy

Unaltered, altered and vein samples were collected at the Virgin, Mitchel-Sheba and Lone Star occurrences (see Appendix A for a full list of samples). Systematic sampling began with fresh, unaltered host rock collected 5–20 m away from veins. Sampling continued toward the veins, and lightly, moderately and heavily altered samples were collected. Lastly, vein material with adjacent wall rock was sampled. Metamorphic rocks are named with porphyroblastic minerals listed first, followed by major rock-forming minerals (≥5%) in decreasing abundance. Mineral abbreviations are from Kretz (1983).

Whole-rock compositions

Whole-rock chemical analysis was conducted by Bureau Veritas Mineral Laboratories in Vancouver. X-ray fluorescence was used to analyze major elements and inductively coupled plasma mass spectrometry (ICP-MS) was used to analyze lithophile and rare earth elements. A 4-acid digestion with ICP-MS finish was used to analyze other trace elements.

Scanning electron microscope and electron probe micro-analyzer analysis

Scanning electron microscope (SEM) analysis was done at the Electron Microbeam and X-Ray Diffraction Facility at the University of British Columbia. A Philips XL-30 SEM with a Bruker Quantax 200 energy-dispersion X-ray microanalysis system, XFlash 6010 SDD detector, and Robinson cathodoluminescence detector was used to investigate micro-textures, identify unknown minerals, locate monazite, and reveal different generations of quartz veins. Silicon (Si), calcium (Ca), yttrium (Y), Th and U elemental maps of individual monazite grains were produced at the Fipke Laboratory for Trace Element Research at the University of British Columbia Okanagan with a Cameca SXFive Field Emission electron probe micro-analyzer (EPMA) at 15 Kv and 200 nA with a fixed beam, 100 ms dwell time, and 0.5 to 0.1 µm step size.

Monazite U-Th-Pb and trace-element analyses

The complete monazite geochronology dataset, including quantitative concentrations, common Pb-corrected isotope ratios, and calculated dates can be found in Appendix C. Monazite U-Th-Pb and trace-element analyses were conducted in situ by laser ablation (LA)-ICP-MS at the Pacific Centre for Isotopic and Geochemical Research at the University of British Columbia. Ablation spots were selected to avoid grain edges and neighbouring ablation sites. If possible, spots were placed in chemical zones. Two separate analytical procedures, with different laser ablation systems, ablation spot locations, and mass spectrometers, were used to collect U-Th-Pb isotopes and trace element

isotopes (Table 2). Analyses that hit inclusions or where the age uncertainty was >8% (>10% was used at Mitchell-Sheba as monazite grains there are smaller and have higher uncertainty) were omitted.

The U-Th-Pb analyses of monazite were performed using an ArF excimer laser ablation system (ESI-New Wave Research NWR193^{UC}) coupled to a high-resolution ICP-MS instrument (ThermoFinnigan Element2). The grains were analyzed for mass/charge corresponding to isotopes of lead (^{204}Pb, ^{206}Pb, ^{207}Pb, and ^{208}Pb), uranium (^{235}U and ^{238}U), and thorium (^{232}Th), as well as mercury (^{202}Hg) to constrain the isobaric interference of ^{204}Hg on ^{204}Pb. External standardization included bracketing groups of ten unknown monazite analyses with two analyses of the Manangotry monazite (555 ± 1 Ma; Paquette et al., 1994; Horstwood et al., 2003; Paquette and Tiepolo, 2007). The Moacyr monazite (504.3 ± 0.2 Ma; Seydoux-Guillaume et al., 2002a,b; Gasquet et al., 2010) was used as a secondary monitor to ensure the accuracy of the age analyses. Data reduction in Iolite was performed using the VisualAge data reduction scheme (Petrus and Kamber, 2012). After common lead contamination was confirmed by plotting Wetherill (Wetherill, 1956) and Tera-Wasserburg (Tera and Wasserburg, 1972) concordia diagrams, a common lead correction was performed using the method of Andersen (2002). Low ^{204}Pb counts led to this method being used over a conventional ^{204}Pb correction. We only use the ^{208}Pb/^{232}Th dates because of the significant uncertainty in the ^{207}Pb/^{235}U and ^{206}Pb/^{238}U dates of relatively young monazite (Grand'Homme et al., 2016; Scharer, 1984; further discussed in Stroh, 2019).

The trace element analyses of monazite were performed using an ArF excimer laser ablation system (Resonetics RESOlution M-50-LR, ASI Australia) coupled to a quadrupole ICP-MS instrument (Agilent 7700x). The grains were analyzed for mass/charge corresponding to thirty-three isotopes that include the full suite of rare earth elements. External standardization was done by bracketing groups of five unknown monazite analyses with one analysis of the BCR2G glass reference material (Jochum et al., 2005), whereas NIST610 and NIST612 glasses were used as secondary monitors. Because these reference materials are not appropriately matrix-matched to monazite, no internal standardization was used, and data from this procedure are considered to be semi-quantitative.

Table 2. Laser ablation parameters for monazite analysis.

	U-Th-Pb analysis	Trace element analysis
Wavelength	193 nm	193 nm
Spot diameter	10 µm	19 µm
Energy density	3 J/cm^2	2 J/cm^2
Repetition rate	8 Hz	8 Hz
Ablation time	25 s	40 s
Gas blank time	30 s	20 s

Monazite characterization

We used several petrographic and trace element parameters to help determine whether monazite dates record hydrothermal or metamorphic crystallization (Table 1). First, each sample was classified according to its relationship to a vein and assigned an alteration intensity, as summarized in Figure 1. Each grain was also assigned one of four petrographic associations (Fig. 1): 1) adjacent to muscovite-quartz, which is the typical petrographic setting of monazite grains with ambiguous origins; 2) aligned in the schistosity, which indicates the monazite grain may have grown during metamorphism or hydrothermally precipitated along the planar features; 3) adjacent to a fracture, which may indicate the monazite grain precipitated hydrothermally along the fracture; and 4) adjacent to pyrite, which may indicate the monazite grain precipitated hydrothermally, given that pyrite is typically a hydrothermal mineral in the Klondike (aside from the pre-existing pyrite phase in the disseminated Au zone at Lone Star [MacKenzie et al., 2008b]). Additionally, we considered the grain shape (from anhedral to euhedral); grain form factor (4π[area]/√[perimeter]), which is a proxy for grain irregularity where values approaching 1 indicate more equant shapes; the grain cross-sectional area; the grain aspect ratio (major axis/minor axis); the grain compactness (√[4area/π]/major axis); and the grain roundness (4area/π√[major axis]). We integrated the petrographic data with monazite ^{208}Pb/^{232}Th dates, ThO_2 concentration, U/Th, Eu anomaly ($Eu/Eu^* = Eu_N/\sqrt{[Sm_N \times Gd_N]}$; used as a proxy for equilibration with plagioclase and apatite), Gd/Yb (used as proxy for equilibration with garnet and apatite), and Ca concentration (used as a proxy for the component of Ca-rich monazite varieties brabantite and cheralite).

Results

Petrography and vein textures

The Klondike schist comprises a spectrum of felsic (Figs. 3a and 5a) to mafic (Fig. 4a) rock types. The host rock mineralogy for the Virgin, Mitchell-Sheba, and Lone Star occurrences are summarized in Table 3. The rocks exhibit a penetrative schistosity defined by the alignment of micas and alternating mica-rich and quartz-feldspar-rich layers (Fig. 3b). An overprinting crenulation cleavage is locally observed where micas are abundant (Fig. 3b).

Gold mineralization occurs in all subunits of the Klondike schist (Fig. 2). Gold-bearing quartz veins in the Klondike schist consist almost entirely of quartz (>98%) with minor pyrite (<2%) and trace galena (Table 3). Trace vein phases vary by occurrence and include carbonate, muscovite, chlorite, barite, rutile and chalcopyrite. Gold typically occurs with pyrite along vein margins. The alteration is typically quartz-muscovite-pyrite, and accessory phases including chlorite, carbonate, monazite, rutile, gold, barite, galena and chalcopyrite. There are minor to significant variations of this alteration assemblage that depend

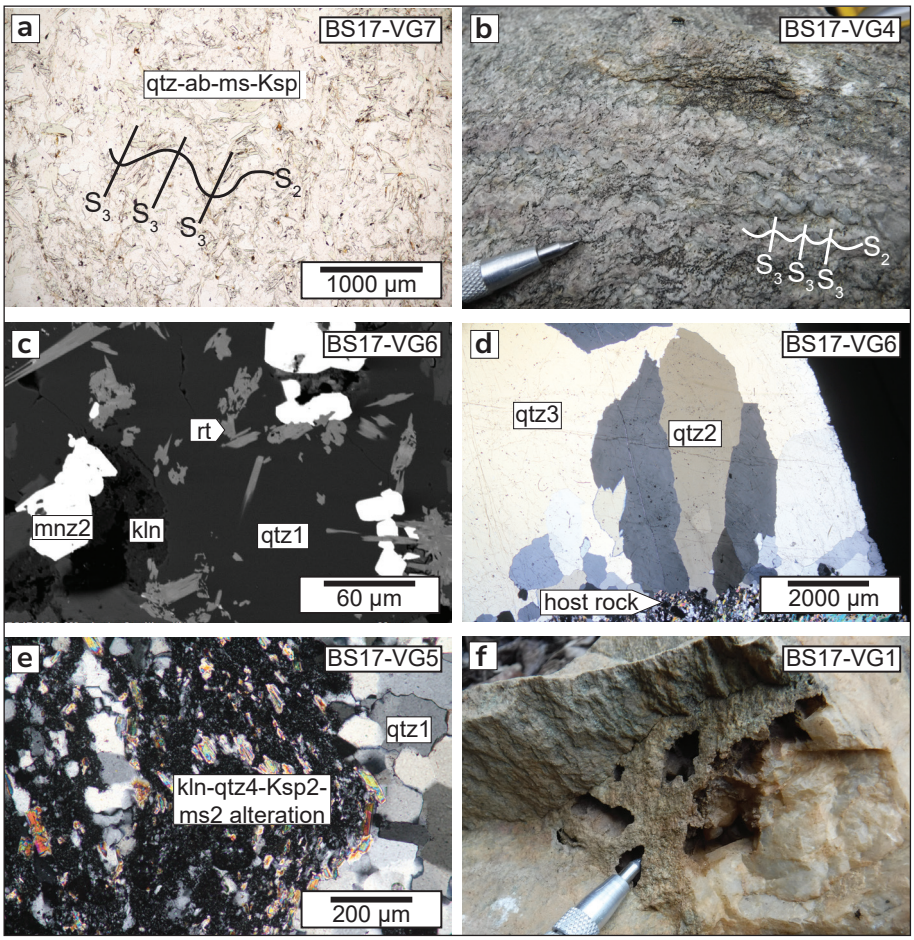

Figure 3. *Hand sample, microscope, and backscattered electron (BSE) images displaying petrographic relationships of the Virgin gold occurrence. Figures (a), (b) and (e) are from the host rock, whereas (c), (d) and (f) are from vein material. Mineral generation numbers are linked to those in Figure 10.* ***(a)*** *Unaltered quartz ± albite-augen quartz-albite-muscovite ± K-feldspar schist with overprinting ductile deformation fabrics (plane polarized light [PPL]; S2 - schistosity, S3 - crenulation).* ***(b)*** *Overprinting ductile deformation fabrics (hand sample).* ***(c)*** *Alteration showing monazite2, rutile and kaolinite (BSE).* ***(d)*** *Syntaxial quartz2 growth from the wall rock, and blocky quartz3 (cross-polarized light [XPL]).* ***(e)*** *Pervasive kaolinite-quartz4-Kfeldspar2-muscovite2 alteration of the wall rock (XPL).* ***(f)*** *Vugs along a vein boundary indicating weathered out pyrite and carbonate (hand sample). Mineral abbreviations: ab – albite; kln – kaolinite; Ksp – K-feldspar; mnz – monazite; ms – muscovite; qtz – quartz; rt – rutile.*

on the local host rocks (Table 3). Gold-bearing quartz vein orientations range from sub-concordant to perpendicular to the wall-rock schistosity. Two different vein textures are observed petrographically (Fig. 3d): 1) elongate, euhedral quartz that grew syntaxially from the wall rock, and 2) blocky quartz that comprises the majority of vein material (Stroh, 2019). These earlier quartz textures were later deformed and partially recrystallized (Fig. 5b). Post-vein deformation features range from subtle kinks of wall-rock fabric to incipiently boudinaged veins (Fig. 6), to boudinaged veins with extensively sheared alteration halos. Microstructures such as undulose extinction, deformation bands, grain boundary migration, and sub-grain rotation in vein-forming quartz also indicate varying degrees of post-vein deformation. Vein quartz has dark, nearly homogeneous cathodoluminescence responses that yield little additional textural information (Stroh, 2019). Brittle fractures, locally filled with carbonate and sparse galena, cross-cut the veins but only rarely propagate into the wall rock (Fig. 4b). Vugs indicate weathering out of carbonate and pyrite in the veins and adjacent wall rock (Fig. 3f).

Virgin

Quartz veins at Virgin are hosted in quartz ± albite-augen, quartz-albite-muscovite ± K-feldspar schist (Fig. 3a). Mortensen (1996) and Mortensen et al. (2019) included these rocks in the quartz-augen schist subunit

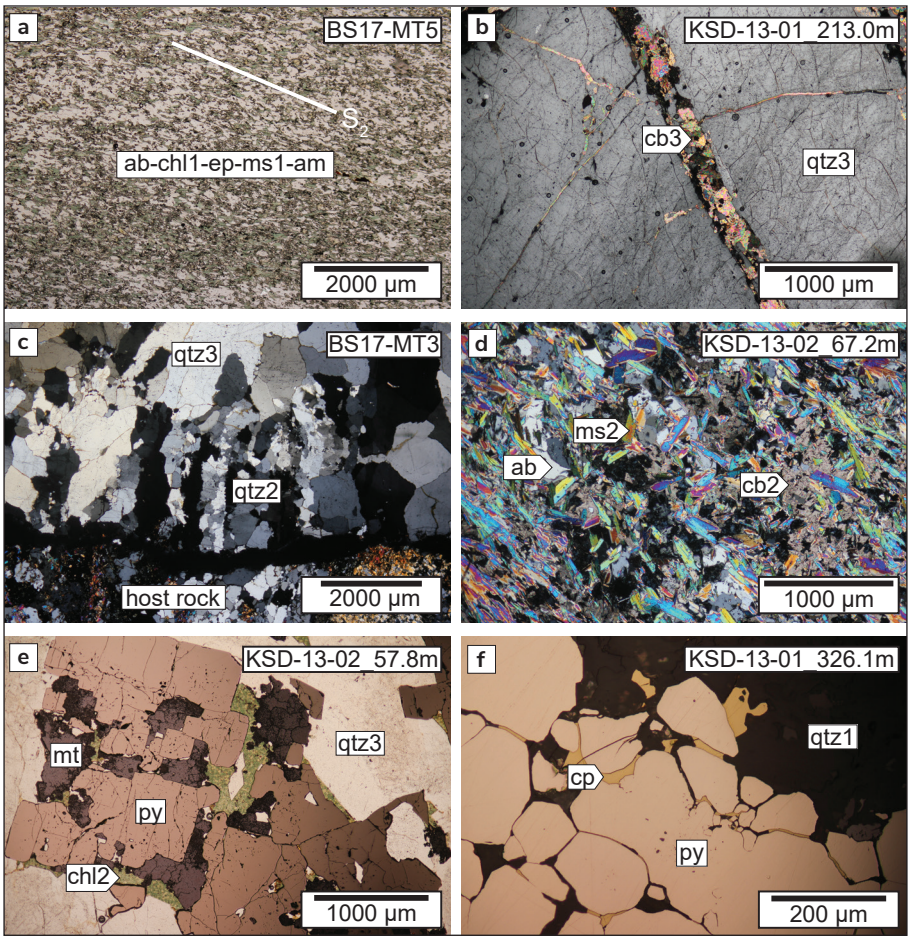

Figure 4. *Microscope images displaying petrographic relationships of the Mitchell-Sheba gold occurrence. Figures (a) and (d) are from the host rock, whereas (b), (c), (e) and (f) are from vein material. Mineral generation numbers are linked to those in Figure 10.* ***(a)*** *Unaltered albite-chlorite-epidote-muscovite ± carbonate ± quartz ± amphibole schist (PPL; S2 - schistosity).* ***(b)*** *Carbonate3 infilling late brittle fractures within a quartz3 vein (XPL).* ***(c)*** *Stretched quartz2 indicating ataxial vein growth and later blocky quartz3 (XPL).* ***(d)*** *Pervasive muscovite2 and carbonate2 alteration (XPL).* ***(e)*** *Pyrite replacing magnetite (reflected light [RL]).* ***(f)*** *Chalcopyrite infilling brittle fractures in pyrite (RL). Mineral abbreviations as in Figure 3; am – amphibole; cb – carbonate mineral; chl – chlorite; cp – chalcopyrite; mt – magnetite; and py – pyrite.*

of the Klondike schist (Fig. 2), which is interpreted to be a hypabyssal equivalent of the metamorphosed felsic volcanic rocks. Quartz ± albite-augen makes up 5–10% of the rock and are surrounded by a finer-grained groundmass of quartz (40%), albite (20%) and muscovite (20%; Table 3). Minor phases (<5%) include K-feldspar, kaolinite and carbonate, whereas trace phases (<<1%) include monazite, zircon and xenotime. The veins at Virgin consist almost entirely of quartz with minor to trace pyrite, muscovite, galena and barite (Table 3). Wall-rock alteration adjacent to the veins is dominated by very fine-grained kaolinite, quartz and K-feldspar with other minor to trace phases, including pyrite, rutile, barite, monazite, and muscovite (Fig. 3e).

Mitchell-Sheba

Quartz veins at Mitchell-Sheba are hosted in fine-grained, albite-chlorite-epidote-muscovite ± carbonate ± quartz ± amphibole schist (Fig. 4a). Mortensen (1996) and Mortensen et al. (2019) included these rocks in the mafic schist subunit of the Klondike schist (Fig. 2). Albite is abundant in the rock (up to 50%), with lesser chlorite (~25%), epidote (~10%) and muscovite (~5%; Table 3). Minor phases include carbonate, quartz, pale-green amphibole and magnetite, whereas trace phases include biotite, K-feldspar, apatite, titanite and zircon. The veins consist almost entirely of quartz, with minor to trace pyrite, muscovite, carbonate, chlorite, rutile and galena (Table 3). Syntaxial quartz growth is not apparent in veins at Mitchell-Sheba. Instead, quartz grains are elongated perpendicular to the vein and do not show growth competition, consistent with ataxial growth (Fig. 4c). Alteration adjacent to the veins is muscovite-carbonate dominated, including chlorite, pyrite and iron alteration of pre-existing chlorite, muscovite and amphibole (Fig. 4d). Pyrite occurs as replacement rims around magnetite (Fig. 4e) and as finely disseminated grains throughout altered wall rock. Trace alteration phases include rutile, galena, chalcopyrite, monazite, arsenopyrite, sphalerite, xenotime and ilmenite. Rutile, arsenopyrite and galena occur as inclusions in pyrite, whereas chalcopyrite and galena occur within fractures in pyrite and quartz (Fig. 4f).

Lone Star

Quartz veins at Lone Star are hosted in quartz-muscovite-albite-chlorite schist (Fig. 5a). Mortensen (1996) and Mortensen et al. (2019) included these rocks in the felsic schist subunit of the Klondike schist (Fig. 2). Quartz dominates the host rock (~50%), and lesser amounts of muscovite (~25%), albite (~15%) and chlorite (~10%) make up the remaining bulk (Table 3). Chlorite is dominantly aligned in the schistosity but locally forms porphyroblasts that have been partially to entirely replaced by carbonate (Fig. 5c). Unlike in the rest of the Klondike, pyrite occurs in relatively high abundance (~1%) and is aligned in the schistosity and crenulation (Fig. 5d; the disseminated Au zone of Mackenzie et al., 2008b). Trace host-rock phases include barite, apatite, monazite and rutile. The veins at Lone Star consist almost entirely of quartz with minor to trace pyrite, carbonate, barite, galena and

Table 3. Summary of petrographic investigations. Minerals are divided into rock-forming minerals, accessory minerals, as well as sulphides and gold. Minerals for each category are listed from most abundant (left) to least abundant (right). Mineral abundances are shown for the unaltered host rock, altered host rock, and vein material of the Virgin, Mitchell-Sheba, and Lone Star gold occurrences. Symbols: * = trace; ** = trace to <2%; *** = ≥2% to <5%; X = ≥5% to <10%; XX = ≥10% to <30%; XXX = ≥30% to <50%; XXXX = ≥50%. Mineral abbreviations: Ab – albite; Am – amphibole; Ap – apatite; Apy – arsenopyrite; Bt – biotite; Brt – barite; Cb – carbonate mineral; Cp – chalcopyrite; Chl – chlorite; Ep – epidote; Gn – galena; Ilm – ilmenite; Kfs – K-feldspar; Kln – kaolinite; Mt – magnetite; Ms – muscovite; Mnz – monazite; Py – pyrite; Qtz – quartz; Rt – rutile; Ser – sericite; Sp – shalerite; Ttn – titanite; Xtm – xenotime; and Zrn – zircon.

Rock type	Rock-forming minerals									Accessory minerals											Sulphides and gold					
	Qtz	Ab	Ms	Chl	Cb	Ep	Kfs	Am	Bt	Kln	Brt	Ser	Rt	Ap	Mt	Mnz	Zrn	Xtm	Ttn	Ilm	Py	Gn	Cp	Sp	Au	Apy
Virgin																										
host rock	XXX	XX	XX		***		X			***		**				*	*	*								
altered host rock	XXX		*				X			XXXX	**		**			*					***				*	
vein	XXXX		**								*										**	*				
Mitchell-Sheba																										
host rock	***	XXX	X	XX	***	XX	**	***	**			**		**	**		*		*							
altered host rock			XXXX	X	XXX								**			*		*		*	***	**	**	*	*	*
vein	XXXX		**	*	**								*								**	*				
Lone Star																										
host rock	XXX	XX	XX	X	X						**	**	*	*		*					**					
altered host rock	XXXX			**	X						**		**			*					***	*	*	*	*	
vein	XXXX				**						**										**	*	*			

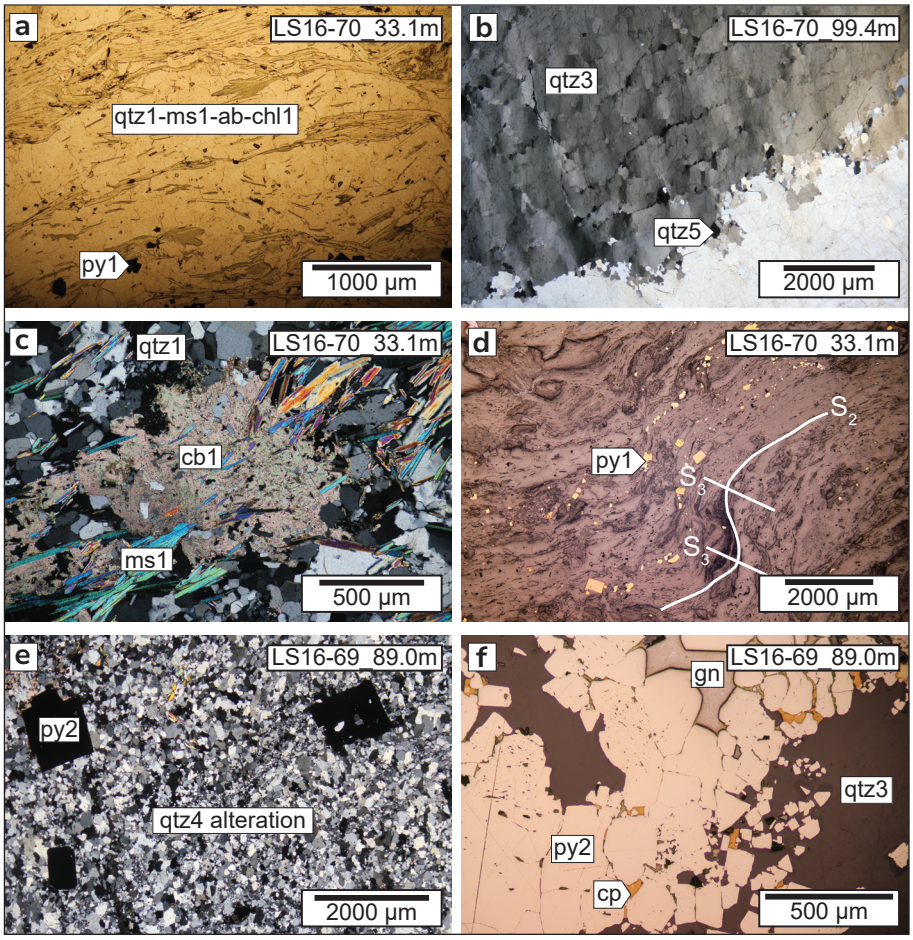

Figure 5. *Microscope images displaying petrographic relationships of the Lone Star gold occurrence. Figures (a), (c), (d) and (f) are from the host rock, whereas (b) and (f) are from vein material. Mineral generation numbers are linked to those in Figure 10.* ***(a)*** *Unaltered quartz-muscovite-albite-chlorite schist (PPL).* ***(b)*** *Blocky vein quartz3 showing ductile deformation in the form of undulose extinction and subgrain rotation (XPL); subgrains rotate to recrystallize and form quartz5.* ***(c)*** *Chlorite porphyroblast replaced by carbonate1 (XPL).* ***(d)*** *Pyrite1 aligned with the schistosity (RL; S2 – schistosity, S3 – crenulation).* ***(e)*** *Pervasive quartz4-pyrite2 alteration (XPL)* ***(f)*** *Galena and chalcopyrite infilling brittle fractures in pyrite indicating they are late in the hydrothermal sequence (RL). Mineral abbreviations as in Figures 3 and 4; gn – galena.*

chalcopyrite (Table 3). Syntaxial quartz vein growth is absent at Lone Star but may have been overprinted by later ductile deformation (Fig. 5b). Wall-rock alteration from the veins is relatively weak and consists mainly of quartz and pyrite (Fig. 5e). Minor to trace alteration phases include carbonate, chlorite, barite, rutile, monazite, galena, chalcopyrite and sphalerite. Galena and chalcopyrite occur within fractures in pyrite and quartz (Fig. 5f). Sub-concordant veins at Lone Star generally have the same vein and alteration assemblage as discordant veins, but locally have more carbonate and chlorite along vein margins, as well as weaker alteration.

Whole-rock lithogeochemistry

On the modified Zr/Ti versus Nb/Y diagram of Pearce (1996; after Winchester and Floyd, 1977), Virgin samples plot in the rhyolite field, Lone Star samples plot across the boundary of the rhyodacite/dacite and andesite fields, and Mitchell-Sheba samples plot in the andesite/basalt field (Fig. 7). No distinct differences exist between unaltered and altered rocks of the same lithology. The complete whole-rock lithogeochemistry dataset can be found in Appendix B.

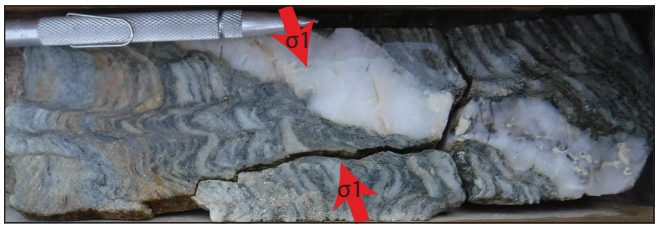

Figure 6. *Locally well-developed crenulation in a mica-rich alteration halo adjacent to an incipiently boudinaged vein. The principal stress direction is indicated by the crenulation and vein deformation (σ1).*

Monazite petrography and characterization

Monazite is a typical trace phase in the unaltered rocks investigated at Virgin and Lone Star (Table 3). The grains are anhedral, equant to elongate, and average ~25 µm in length and have rare grains larger than ~60 µm. They are typically adjacent to muscovite and quartz and are locally aligned with the schistosity. Monazite occurs adjacent to pyrite in unaltered rocks at Lone Star. No monazite was observed in the unaltered rocks at Mitchell-Sheba.

Monazite is rare in vein material and occurs in the altered wall rock at each occurrence (Table 3; Fig. 3c). The size and shape of monazite grains is similar in altered and unaltered rock. Grains in altered rock are also adjacent to muscovite and quartz, and are locally aligned with the schistosity. Thus, it can be difficult with petrography alone to determine whether a monazite crystallized during metamorphism or during a later hydrothermal overprint. A hydrothermal origin was more evident where monazite occurs adjacent to fractures, pyrite, or other hydrothermal minerals such as kaolinite at Virgin.

Monazite element mapping

Electron probe micro-analyzer element maps of Th, Y, U, Ca, and Si in monazite reveal subtle to clear zonation patterns that are dominantly patchy or mottled (Fig. 8; Stroh, 2019). The zonation style is consistent across localities, alteration intensities and petrographic settings. The zoned domains are typically smaller than 10 µm. Thorium is the most prominently zoned element, with domains of relatively high and low concentration in most grains. Yttrium zonation is typically more subdued but generally follows the same pattern as Th. The Y maps also show instances where xenotime is grown adjacent to monazite. Uranium is typically homogeneous. Few monazite grains are entirely free of zonation, and even fewer grains display a core and rim with a high Th and Y core. The Ca and Si maps were used to check for apatite and silicate micro-inclusions.

Monazite geochronology

Monazite U-Th-Pb analyses (n=272) yielded $^{208}Pb/^{232}Th$ dates from 189 ± 14 to 116 ± 4 Ma and indicated ThO_2 concentrations from 0.13 ± 0.01 to 7.38 ± 0.13 wt% (Fig. 9; Appendix C). Different spot analyses of zoned grains typically yielded identical dates, the only exception being monazite LS16-69 89.4m-M11 (Stroh, 2019). Monazite dates and ThO_2 concentrations differ between occurrence and petrographic association (Fig. 9). The ThO_2 concentrations and dates show no systematic relationship with other parameters, including sample, grain form, grain form factor, grain area, grain aspect ratio, grain compactness, grain roundness, U/Th ratio and trace element composition.

The analyses from Virgin yielded dates from 185 ± 14 to 117 ± 4 Ma and ThO_2 concentrations from 0.32 ± 0.02 to 7.38 ± 0.13 wt% (Fig. 9). Our results reveal two distinct populations: a relatively old and ThO_2-rich (>2.00 wt%) population (n = 16) in dominantly unaltered samples, and a relatively young ThO_2-poor (<2.00 wt%) population (n = 32) in altered

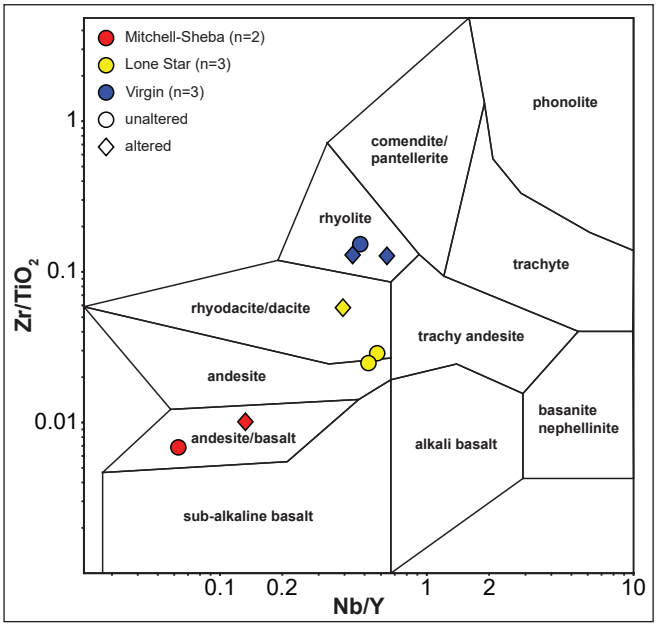

Figure 7. *Modified Winchester and Floyd (1997) diagram of Pearce (1996). Whole-rock lithogeochemistry samples from the Klondike are plotted and coloured based on locality. Lone Star samples are from Nugget but represent the host rock at Lone Star, 1.8 km away. Mitchell-Sheba samples are from Mitchell but represent the same host rock at Sheba, 850 m away. Mitchell-Sheba: mafic protolith; Lone Star: intermediate protolith; Virgin: felsic protolith.*

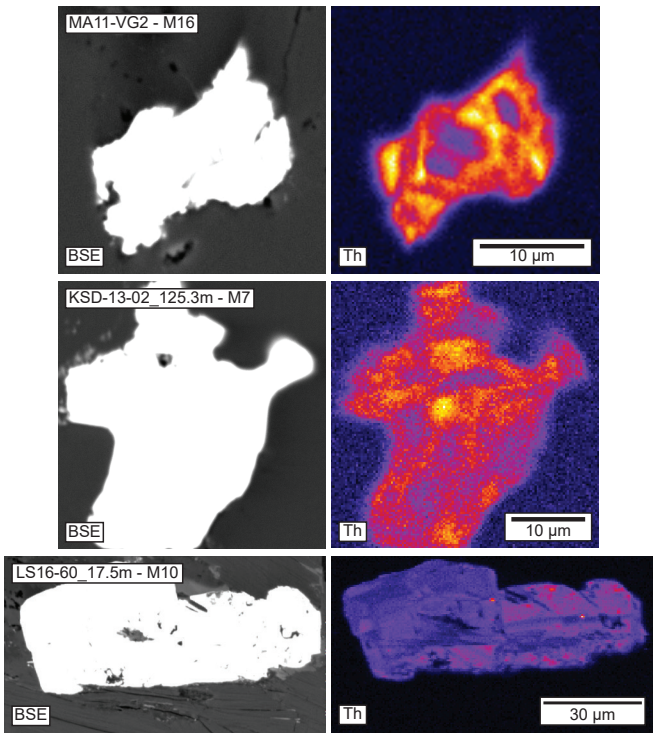

Figure 8. *Representative monazite backscattered electron and element maps. Thorium maps are displayed because they show the most visible zonation.* ***Top:*** *Monazite MA11-VG2-M16 from a vein/wall-rock sample at Virgin displays mottled zonation. The grain is surrounded by vein quartz and interpreted as hydrothermal.* ***Middle:*** *Monazite KSD-13-02 125.3m-M7 from a heavily altered sample at Mitchell-Sheba displays mottled zonation. The grain is adjacent to quartz and is interpreted as hydrothermal.* ***Bottom:*** *Monazite LS16-69 17.5m-M10 from a vein/wall-rock sample at Lone Star displays patchy/mottled zonation. The grain is aligned in the schistosity and may have been reset by hydrothermal fluids.*

samples and grains adjacent to pyrite. Monazite that is adjacent to pyrite (n = 12) yielded dates from 178 ± 6 to 122 ± 7 Ma and ThO_2 concentrations ≤1.80 wt%. The analyses from Mitchell-Sheba yielded dates from 175 ± 13 to 126 ± 8 Ma and ThO_2 concentrations from 0.16 ± 0.01 to 1.57 ± 0.15 wt% (Fig. 9). Monazites adjacent to pyrite (n = 6) yielded dates from 171 ± 14 to 140 ± 13 Ma and ThO_2 concentrations ≤1.57 wt%. The analyses from Lone Star yielded dates from 189 ± 14 to 116 ± 4 Ma and ThO_2 concentrations from 0.13 ± 0.01 to 5.33 ± 0.16 wt% (Fig. 9). There are no clear relationships between date, ThO_2 concentration, grain form, and sample alteration intensity. Grains that are aligned in the schistosity are generally older, whereas the grains adjacent to pyrite are younger, though significant overlap exists. Monazites that are aligned in the schistosity (n = 74) yielded dates from 189 ± 8 to 144 ± 8 Ma and ThO_2 concentrations ≤4.31 wt%. Monazites that are adjacent to pyrite (n = 50) yielded dates from 178 ± 8 to 116 ± 4 Ma and ThO_2 concentrations ≤3.97 wt%.

Monazite trace-element analyses

A total of 90 analyses yielded Gd/Yb values of 21 to 315 and Eu/Eu* of 0.31 to 1.09 (Stroh, 2019). The values for Gd/Yb and Eu/Eu* exhibit a (arguably) weak inverse relationship at Lone Star, whereas no relationship is observed in the relatively small dataset for Virgin. Neither Gd/Yb nor Eu/Eu* correlate with grain form, grain form factor, grain area, grain aspect ratio, grain compactness, grain roundness, date, or ThO_2 concentration. Trace-element analyses were not conducted at Mitchell-Sheba as grains were too small for the required 19 µm spot size. The Ca content of analyzed monazite is uniform and does not reveal distinct populations or trends.

Discussion

Vein formation and overprinting deformation

Quartz veins in the Klondike were previously interpreted to form in two distinct generations: early, barren metamorphic segregation veins, and late, gold-bearing discordant veins that were purely brittle (MacKenzie et al., 2008a). Based on our observations, we developed a paragenetic summary (Fig. 10) with evidence of protracted vein formation in the brittle-ductile transition zone, and ongoing ductile deformation after vein emplacement. Quartz vein textures indicate at least two stages of formation. The first is indicated by epitaxial quartz growth near vein boundaries that suggest multiple crack-seal events (Qtz2; Figs. 3d and 4c). The second stage of vein formation is indicated by blocky quartz grains that compose most of the veins (Qtz3; Figs. 3d and 4c). The blocky texture suggests at least one additional crack-seal event, where the dilation rate exceeded crystal growth, allowing quartz growth into free space (Hilgers et al., 2001). Although Klondike veins were previously thought to have formed in a single stage (MacKenzie et al., 2008a), vein textures here display evidence of multiple crack-seal events, in agreement with Wolff (2012). The early vein formation as narrow epitaxial growths before wider open space filling suggests increasing strain rates over time.

Different degrees of overprinting deformation presented above suggests that veins formed during progressive to brittle-ductile deformation. Vein

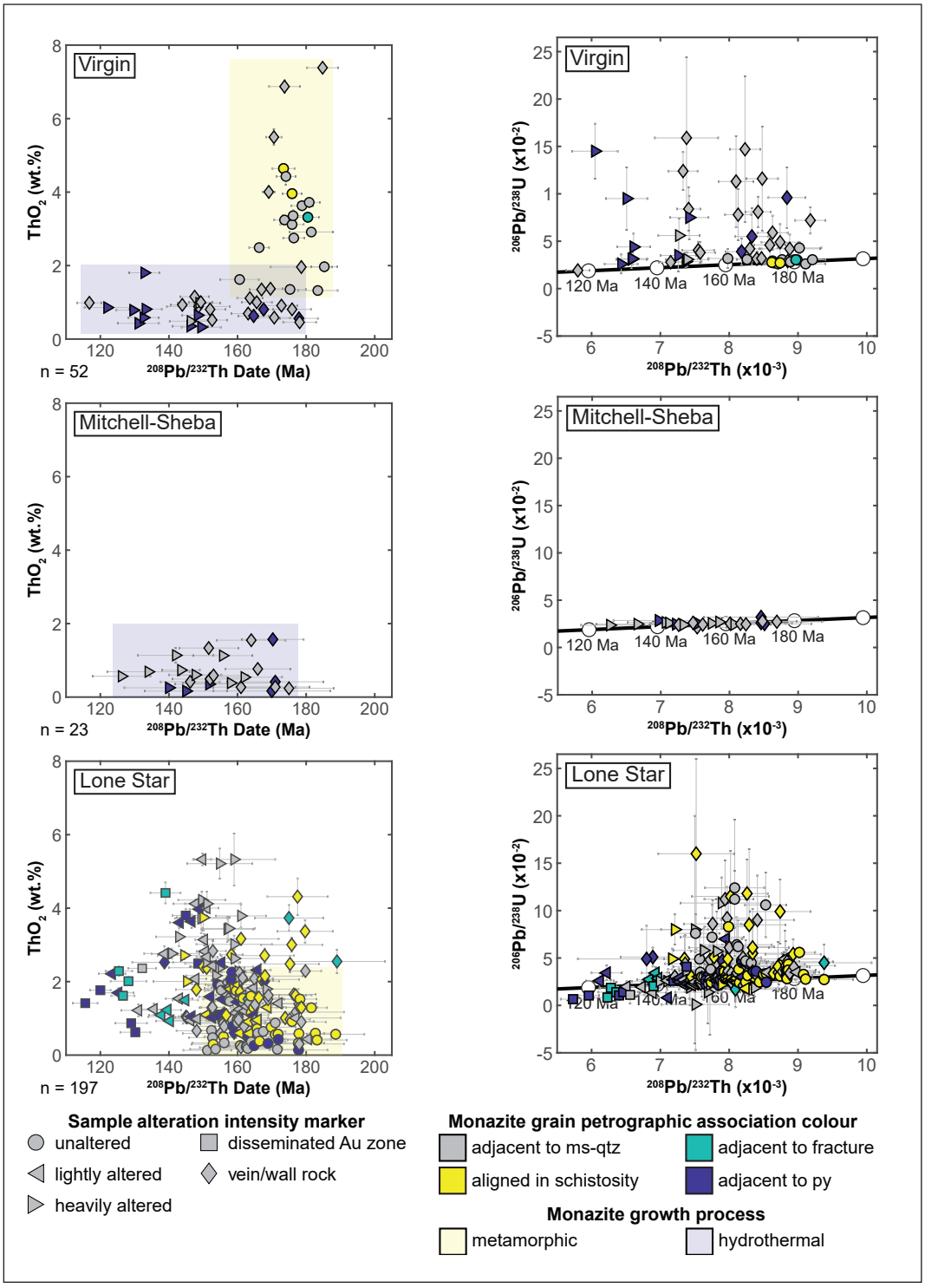

Figure 9. *Monazite geochronology results and growth process interpretations. Each data point represents one LA-ICP-MS analysis. Thin grey lines represent uncertainty in 2σ. Where no uncertainty line is visible, the uncertainty is less than the size of the marker. Multiple samples are shown on the same diagram, and thus the marker shape is dictated by the sample alteration intensity. Marker colour is based on the monazite grain petrographic association.* ***Left:*** *ThO_2 vs. date plots.* ***Right:*** *U-Th-Pb concordia diagrams.* ***Top:*** *Results from Virgin.* ***Middle:*** *Results from Mitchell-Sheba.* ***Bottom:*** *Results from Lone Star. Ms-qtz – muscovite-quartz; py – pyrite.*

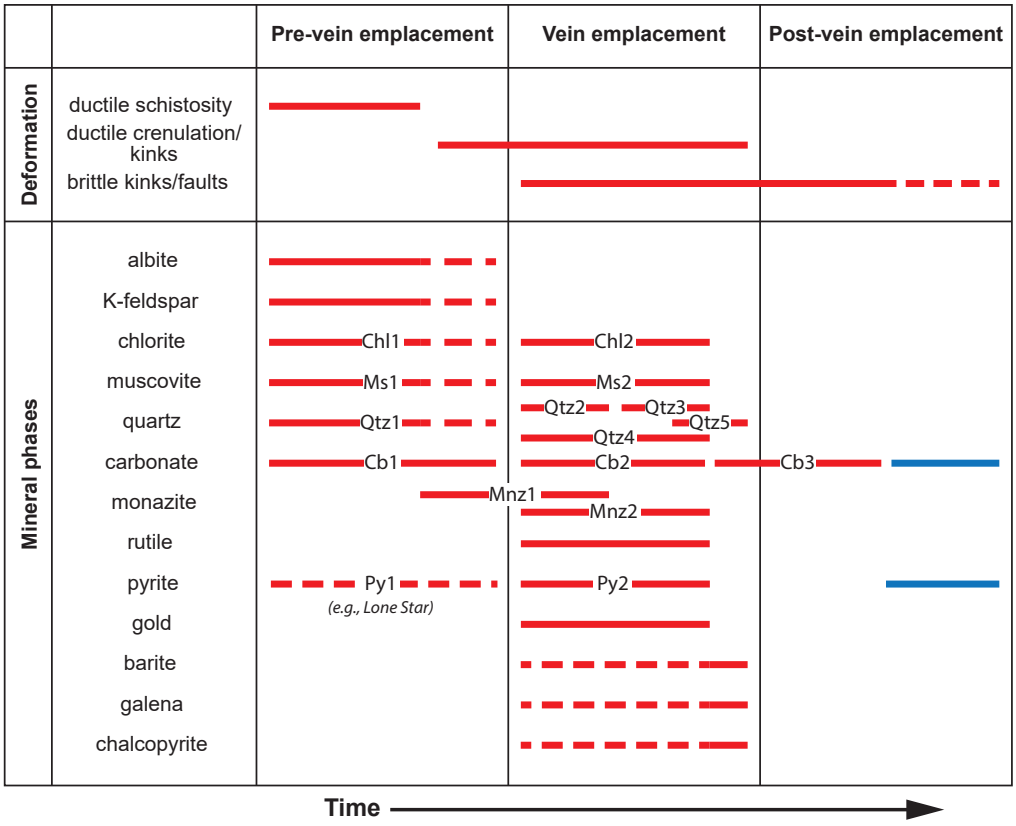

Figure 10. *Simplified paragenesis chart for the Klondike gold occurrences based on petrographic and cathodoluminescence analysis of 37 polished thin sections from the Virgin, Mitchell-Sheba and Lone Star gold occurrences. Red represents phase formation, whereas blue indicates break down by oxidation or weathering. Chl1: metamorphic/recrystallized; Chl2: host alteration; Ms1: metamorphic/recrystallized; Ms2: host alteration; Qtz1: metamorphic/recrystallized; Qtz2: syntaxial vein filling; Qtz3: blocky vein filling; Qtz4: host alteration; Qtz5: dynamic recrystallization of pre-existing vein quartz; Cb1: metamorphic/recrystallized; Cb2: infrequent vein filling/host alteration; Cb3: fracture filling; Mnz1: metamorphic/recrystallized; Mnz2: host alteration. Metamorphic minerals are solid then dashed because most of the mineral growth is interpreted to occur during schistosity formation, but some may be related to the crenulation forming event. Metamorphic carbonate (Cb1) is not dashed because it locally replaces pre-existing, metamorphic chlorite (Chl1; Figure 5c). Barite, galena and chalcopyrite begin dashed because they can be included in quartz and pyrite but are typically late in brittle fractures. Brittle fracturing likely continued during exhumation and weathering and is dashed.*

orientations ranging from sub-concordant to discordant to the wall-rock schistosity as well as macro and micro-structural evidence suggest at least some level of ductile deformational overprinting and local dynamic recrystallization of all vein generations (e.g., Figs. 3d and 4c). Deformation fabrics are locally strong within micaceous vein alteration haloes, suggesting a relative timing whereby vein emplacement and host-rock alteration occurred prior to deformation (Fig. 6). Late in the deformation sequence, carbonate veinlets filled brittle fractures in quartz veins (Fig. 4b) but rarely propagated into the host rock, indicating that the more competent vein-filling quartz behaved brittlely, whereas micaceous wall rock accommodated strain in a ductile manner. Vein quartz investigation by cathodoluminescence indicates dark, nearly homogeneous responses (Stroh, 2019), which agrees with Rusk's (2012) description of recrystallized quartz in orogenic settings.

The exact timing of gold precipitation relative to vein formation and deformation remains ambiguous as gold-bearing veins are overprinted by various amounts of deformation. Limonitic selvages along folded vein margins commonly host gold (Rushton et al., 1993) and suggests that mineralization occurred prior to ductile

deformation. However, Grimshaw (2018) describes a late, brittle deformation stage of gold precipitation at Lone Star, implying that gold was locally introduced or remobilized late in the deformation sequence. This evidence suggests that the timing of gold precipitation in the Klondike may span the timing of vein formation or vary locally by occurrence.

Linking monazite dates with petrographic associations and geochemistry

Our results reveal monazite crystallization from ca. 190 to 120 Ma, a time span of ~70 m.y. (Fig. 9). These dates are considerably younger than the 269 to 253 Ma age of the Klondike assemblage protolith (Colpron et al., 2006) and also coincide with a regional magmatic gap from 179 to 115 Ma (Allan et al., 2013). Thus, we rule out the presence of igneous grains in our dataset and interpret all the dates as either metamorphic or hydrothermal. To discriminate between hydrothermal and metamorphic crystallization we integrated the dates with the petrographic and geochemical parameters summarized in Table 1. We interpret that monazite from unaltered samples is metamorphic, as they are apparently beyond the influence of hydrothermal alteration. Monazite aligned in the schistosity is commonly but not always metamorphic; hydrothermal monazite may have preferentially formed along these planar features.

Petrographic relationships and ThO_2 concentrations of monazite were the most useful parameters for differentiating hydrothermal and metamorphic crystallization. The monazite trace-element data generally lacks discernable relationships to help distinguish growth mechanisms and is interpreted in greater detail in Stroh (2019). The REE composition may help to distinguish hydrothermal (no Eu anomaly; precipitated without plagioclase) from metamorphic (negative Eu anomaly; grew in contact with plagioclase) monazite grains, but petrographic support for this is absent. Similarly, the relationship between Gd/Yb and Eu/Eu* suggests local monazite growth with or without coeval apatite and plagioclase, but this relationship does not reliably differentiate between a hydrothermal and metamorphic origin.

Virgin

Our analyses reveal two populations of monazite dates at the Virgin occurrence: an older (185–161 Ma) population with up to 7.38 wt% ThO_2, and a mostly younger (178–117 Ma) population with ≤1.80 wt% ThO_2 (Fig. 9). Although ThO_2 concentrations are variable in metamorphic monazite, concentrations are typically <2 wt% in hydrothermal monazite (Schandl and Gorton, 2004; Kohn and Malloy, 2004; Catlos, 2013). Collectively, the broad range in ThO_2 concentrations and dominance of monazite in unaltered samples suggest the older monazite at Virgin is metamorphic. A hydrothermal origin is supported for the younger population by the alteration extent of the samples, abundance of grains adjacent to pyrite, and the low ThO_2 concentrations. Grains that are adjacent to pyrite, which overprints the schistosity, all have <2 wt% ThO_2. Although metamorphic monazite can have ThO_2 concentrations <2 wt%, we interpret all monazite with >2 wt% ThO_2 as metamorphic.

Mitchell-Sheba

At Mitchell-Sheba, monazite occurs exclusively in the alteration zone surrounding the vein, commonly occurring adjacent to pyrite. All monazite contains <2 wt% ThO_2, consistent with hydrothermal crystallization. We interpret this group to record the same younger population at Virgin, further bracketing hydrothermal monazite growth between 175 and 126 Ma. The lack of metamorphic monazite is unsurprising given the mafic composition of the host rock (Fig. 7). Whole-rock compositional data from the three occurrences are shown in Figure 11. Higher Zr/TiO_2 ratios indicate more felsic host rocks. The felsic host rock at Virgin is the most enriched in incompatible elements, including Th, thus allowing more Th to be available to metamorphic monazite. The intermediate rock at Lone Star is lower in incompatible elements, including Th, which limits both the growth of metamorphic monazite and its Th concentration. The mafic host rock at Mitchell-Sheba has the lowest Th and cerium (Ce) concentrations, which explains the lack of metamorphic monazite. The felsic host rocks were also more likely to have abundant primary apatite, a precursor to metamorphic monazite, whereas apatite would likely have been absent in the mafic host rocks (Overstreet, 1967). Therefore, not only does the variable ThO_2 concentration of metamorphic monazite increase with increasing grade (Schandl and Gorton, 2004), but it also depends on the composition of the protolith. Under the greenschist metamorphic conditions of the Klondike, monazite develops with 0.13 to 7.38 wt% ThO_2, but is typically <5 wt%. Rocks with a mafic protolith produce no monazite under these conditions, whereas rocks with an intermediate protolith produce monazite with 0.13 to 2.26 wt% ThO_2, and rocks with a felsic protolith produce monazite with 1.32 to 7.38 wt% ThO_2.

Lone Star

The relationship between ThO_2 concentration and age in the Lone Star data is more complex than the other two occurrences (Fig. 9). Monazite from unaltered samples yielded dates from 189 to 151 Ma, which bracket the range of metamorphic dates (185–161 Ma) we infer from the Virgin occurrence. However, these monazite grains are characterized by low ThO_2 concentrations (<2 wt%) and commonly occur adjacent to pyrite, indicative of hydrothermal crystallization. Although characteristic of hydrothermal monazite, low thorium concentrations are also common in metamorphic monazite (Schandl and Gorton, 2004), and, as mentioned above, at least some of the pyrite at Lone Star predates vein formation (Fig. 10). Thus, we interpret older monazite grains from unaltered samples at Lone Star as metamorphic (yellow box in Fig. 9). Analyses at Lone Star with relatively young dates (<151 Ma) have highly variable ThO_2 concentrations that include values up to ~5 wt%, consistent with metamorphic crystallization. However, post ca. 160 Ma, metamorphic growth is inconsistent with our data from Virgin. Our preferred interpretation is that the younger, high-Th monazite is metamorphic monazite in which U-Th-Pb systematics were re-equilibrated. This interpretation requires that a hydrothermal fluid reset the dates, while preserving the ThO_2 concentrations of pre-existing metamorphic monazite. Williams et al. (2011) have previously documented this process. The sparse population of grains with older dates (>151 Ma) and high ThO_2 concentrations (>2 wt%) may be metamorphic monazite that retained its primary age signature. The population of young (<151 Ma), ThO_2-poor (<2 wt%) monazite could be a combination of hydrothermal and partially reset metamorphic monazite.

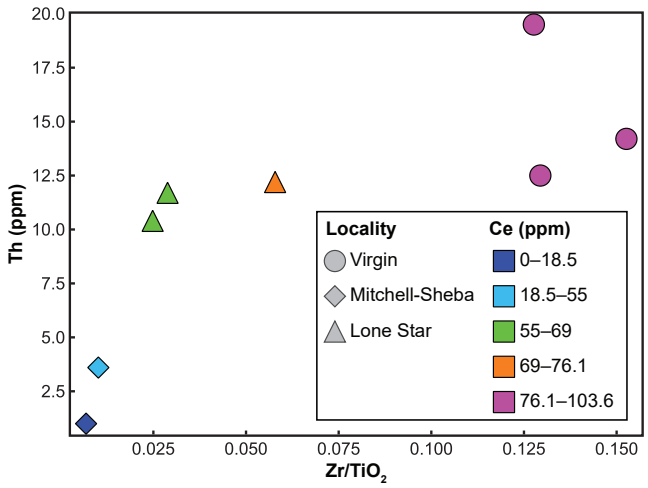

Figure 11. *Whole-rock lithogeochemical data suggesting the host rock composition controls the metamorphic monazite composition. The ratio of Zr/TiO_2 is treated as a measurement from mafic (low) to felsic (high). More felsic host rocks have increasing thorium (Th) and cerium (Ce) concentrations, which translates to metamorphic monazite growth with higher ThO_2 concentration. Mafic rocks do not have metamorphic monazite. Thus, the host-rock composition controls the ThO_2 concentration in metamorphic monazite.*

Linking monazite growth and regional tectonics

Figure 12 presents a compilation of all the monazite dates with their interpreted growth mechanism, as discussed in the previous section. Our results bracket an early (ca. 190–150 Ma) generation of metamorphic monazite followed by a later (ca. 180–120 Ma) population of hydrothermal monazite. Our metamorphic monazite dates align with previously documented evidence for Early–Middle Jurassic deformation and metamorphism of Yukon-Tanana terrane associated with the accretion of the intermontane terranes to North America (Berman et al., 2007; Gaidies et al., 2021; Colpron et al., 2025). The spread of metamorphic dates also coincides with Jurassic cooling ages that record the exhumation of Yukon-Tanana to upper crustal levels (Fig. 13; Joyce et al., 2015; Yukon Geological Survey, 2023), suggesting that monazite growth occurred during prograde and retrograde metamorphism. During exhumation, infiltrating fluids may have facilitated monazite formation through the breakdown of allanite, apatite, or pre-existing monazite (Ayers et al., 2002; Bollinger and Janots, 2006; Finger and Krenn, 2007; Johnson et al., 2015). The dates obtained for hydrothermal monazite (ca. 180–120 Ma) coincide with those obtained for hydrothermal mica, suggesting that vein formation began shortly after the onset of exhumation (Fig. 13; Breitsprecher and Mortensen, 2004; Joyce et al., 2015). The monazite dates indicate that vein formation persisted until after the country rock had cooled through the closure temperature of mica (e.g., ~380°C for muscovite; Reiners and Brandon, 2006), consistent with vein-forming fluid inclusion trapping temperatures of 200 to 350°C (Rushton et al., 1993). We were unable to directly date gold mineralization. The timing of vein formation nevertheless overlaps with an unpublished U-Pb date of 156 ± 8 Ma obtained from hydrothermal rutile in a gold-bearing quartz vein (Mortensen, 2012, in Allan et al., 2013).

In addition to the lengthy timespan of each growth mechanism, our results suggest that hydrothermal and metamorphic monazite growth temporally overlapped for a period of ca. 30 m.y. The large range of monazite dates may in part be due to disturbances of the isotopic U-Th-Pb systematics, highlighted by the evidence of partially reset metamorphic monazite at Lone Star (Fig. 9). Regardless, our data demonstrate that Jurassic regional metamorphism was subsequently followed by Jurassic to Early Cretaceous vein formation and hydrothermal alteration, most likely due to progressive deformation. Evidence of protracted orogenic gold mineralization under similar tectonic circumstances has also been documented in the Cariboo gold district of east-central British Columbia, where vein formation spanned from 155 to 134 Ma during progressive ductile to brittle deformation (Rhys et al., 2009; Mortensen et al., 2011; Allan et al., 2017). Veins that formed early in the deformation sequence are only weakly mineralized and overprinted by ductile deformation, whereas veins that formed later have ore-grade gold values and are only weakly strained to unstrained (Allan et al., 2017). Although the veins formed over 21 m.y., mineralization is interpreted to have lasted 15 m.y., from 149 to 134 Ma (Rhys et al., 2009; Mortensen et al., 2011; Allan et al., 2017). Like the Klondike, veins in the Cariboo district exhibit varying levels of deformation that indicate vein formation progressed as deformation became increasingly brittle.

The protracted time span of vein formation in the Klondike may reflect input from multiple sources. Staples et al. (2016) suggested that amphibolite-facies metamorphism of the Finlayson Lake domain between 169 and 142 Ma led to the release of metamorphic fluids, which travelled into the Klondike assemblage—an assemblage they interpret to have been adjacent the Finlayson Lake domain prior to post Cretaceous dextral displacement along the Tintina fault. The subsequent burial and devolatilization of the Australia Mountain domain from 146 to 118 Ma (Staples et al., 2013) could have provided additional fluids. Finally, vein-forming fluids may have been sourced from the Klondike assemblage itself, through decompression-driven metamorphic devolatilization reactions during regional Jurassic exhumation (Fig. 13; Vry et al., 2010; White et al., 2015). At Lone Star, Grimshaw (2018) demonstrated that most quartz generations are barren and that gold is introduced in a volumetrically minor, late-stage vein filling. Thus, while the different tectono-metamorphic events recorded in the Klondike region had the potential to generate siliceous fluids, gold endowment may have been restricted to one in particular.

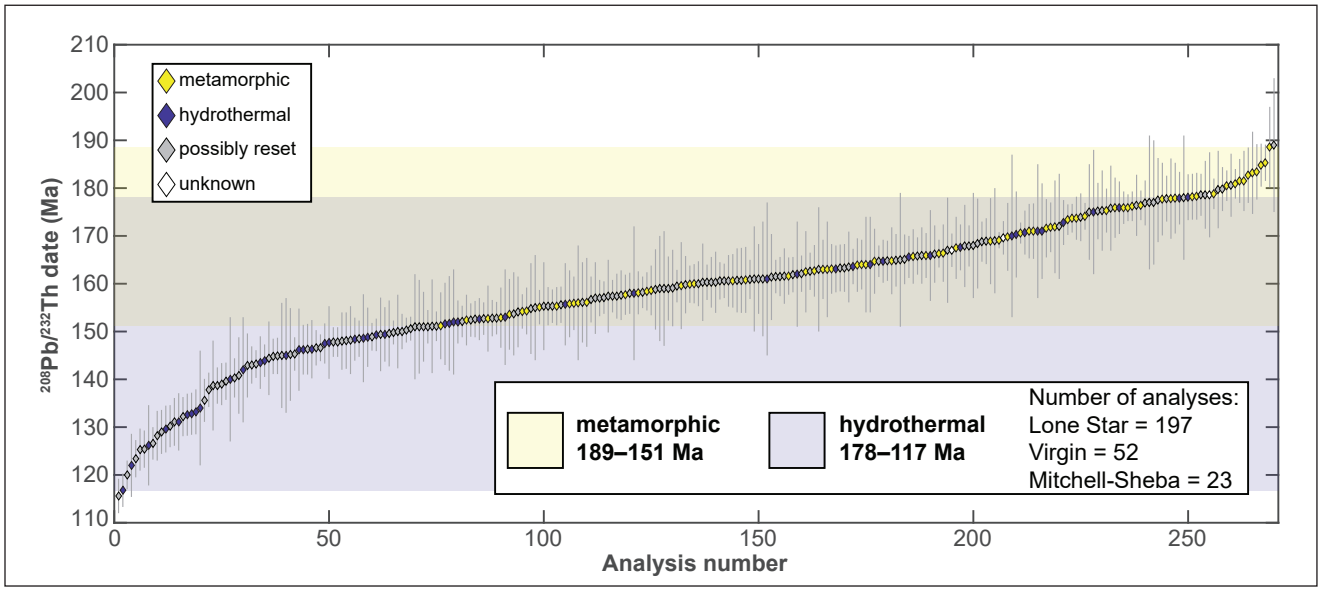

Figure 12. *Summary of all monazite dates in the Klondike and overlain metamorphic and hydrothermal age ranges; grey is overlap. Thin grey lines represent uncertainty in 2σ. Each data point represents one LA-ICP-MS analysis. The marker colour is based on the interpreted growth mechanism that we assigned based on petrographic associations and geochemical (primarily ThO_2 concentration) parameters discussed in the text.*

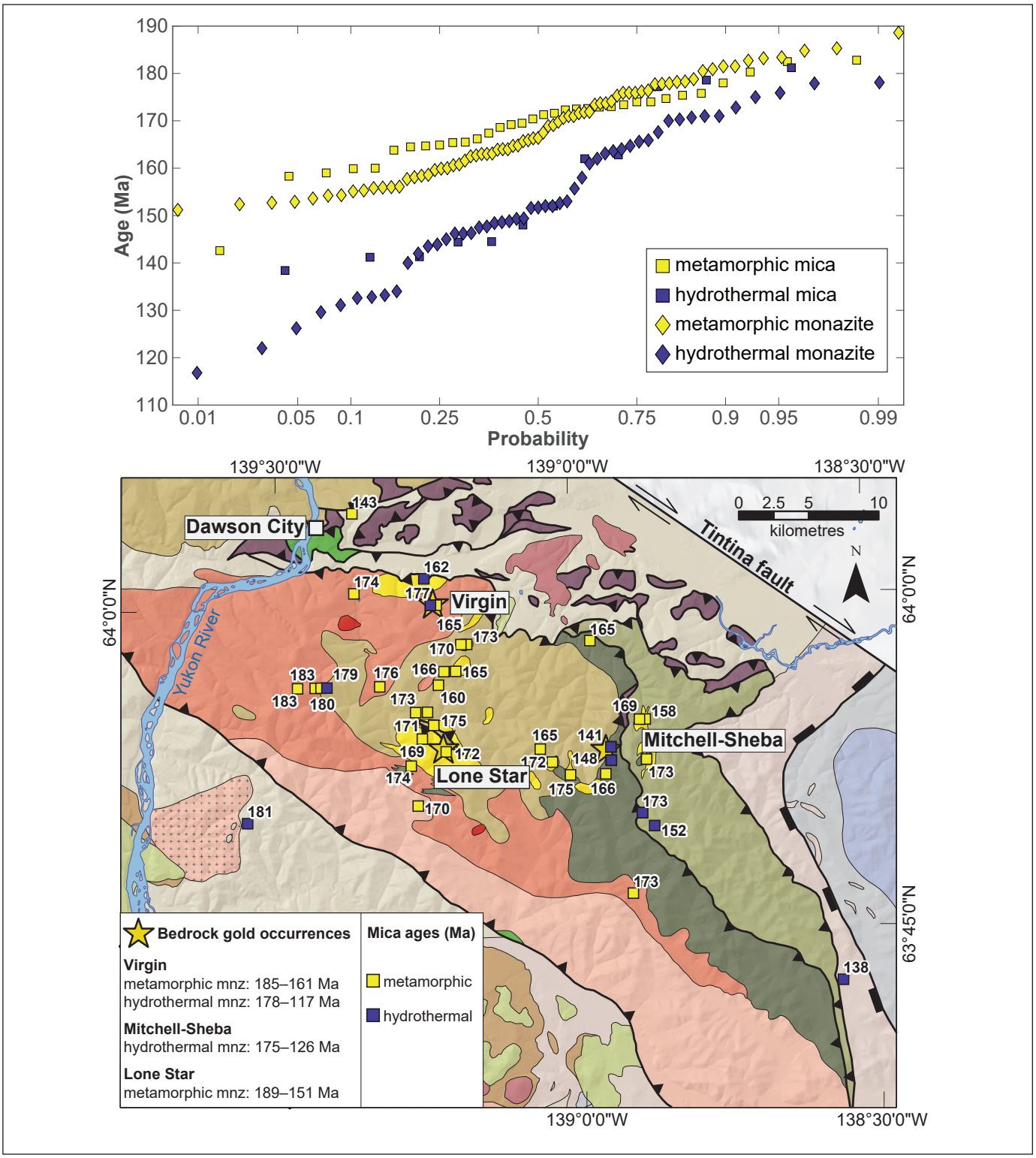

Figure 13. *Comparison of Klondike metamorphic and hydrothermal monazite and mica ages.* ***Top:*** *Split probability plot summarizing the previously published and new metamorphic and hydrothermal ages in the Klondike. The* $^{208}Pb/^{232}Th$ *monazite ages presented herein overlap with previously published* $^{40}Ar/^{39}Ar$ *mica ages. No uncertainty in age is shown for simplicity. Mica ages are from Breitsprecher and Mortensen (2004); Joyce et al. (2015); and unpublished Mineral Deposit Research Unit data. All monazite ages are from this study.* ***Bottom:*** *Geological map of the Klondike summarizing the locations of the ages from the top figure. Monazite age ranges are summarized in the legend. Some mica ages mask others. Legend for geology corresponds to Figure 2.*

Conclusions

The timing of gold mineralization in the Klondike district is constrained by Th-Pb ages of paragenetically related hydrothermal monazite at ca. 180–120 Ma, overlapping with, but generally younger than, an earlier metamorphic monazite population dated at 190–150 Ma. Metamorphic monazite exhibits variable ThO_2 concentrations (0–8 wt% ThO_2) and is prevalent in unaltered rocks distal to orogenic quartz veins. Metamorphic crystallization spanned the burial and subsequent exhumation of the Yukon-Tanana terrane during collision of the Intermontane terranes with North America. In contrast, hydrothermal monazite exhibits low ThO_2 concentrations (<2 wt% ThO_2) and is largely restricted to alteration halos of veins. We were unable to directly link monazite dates to gold mineralization; our inferred timing of vein formation nevertheless overlaps with a previously reported U-Pb date of ca. 156 Ma from hydrothermal rutile in a gold-bearing quartz vein (Mortensen unpublished data, 2012, in Allan et al 2013). Vein-forming fluids likely formed during multiple prograde and retrograde metamorphic events, including regional exhumation (185–140 Ma; Yukon Geological Survey, 2023), Finlayson Lake domain metamorphism (169–142 Ma; Staples, 2014), and Australia Mountain domain metamorphism (146–118 Ma; Staples et al., 2013). Although hydrothermal activity persisted for tens of millions of years, gold mineralization was likely restricted to a significantly shorter time interval. Our monazite dates provide insight into the timing of gold mineralization and reveal the extensive duration and complexity of vein formation in orogenic gold systems.

Acknowledgments

This research was part of the Yukon-Alaska Metallogeny Project based at the Mineral Deposit Research Unit of the University of British Columbia, which was funded by a Natural Sciences and Engineering Research Council of Canada Collaborative Research Development grant, Goldcorp Incorporated (now Newmont Corporation), and Sumac Mines Limited. Additional funds were provided through awards and scholarships, including the Society of Economic Geologists Canada Foundation Graduate Student Fellowship, Northwest Territories and Nunavut Association of Professional Engineers and Geoscientists Finnigan Award for Northern Research, Yukon Foundation Bradshaw Memorial Scholarship, and Plains Midstream Canada Higher Education Award. The authors would like to thank Klondike Gold Corporation, Kestrel Gold Incorporated, and the Yukon Geological Survey for providing access to field sites and drill core. Comments by Patrick Sack and Jim Mortensen on an earlier version of this manuscript led to significant improvements.

References

Allan, M.M., Mortensen, J.K., Hart, C.J.R., Bailey, L.A., Sanchez, M.G., Ciolkiewicz, W., McKenzie, G.G. and Creaser, R.A., 2013. Magmatic and Metallogenic Framework of West-Central Yukon and Eastern Alaska. *In:* Tectonics, Metallogeny and Discovery: The North American Cordillera and Similar Accretionary Settings. M. Colpron, T. Bissig, B.G. Rusk and J.F.H. Thompson (eds.), Society of Economic Geologists Special Publication, vol. 17, p. 111–168.

Allan, M.M., Rhys, D.A. and Hart, C.J.R., 2017. Orogenic gold mineralization of the eastern Cordilleran gold belt, British Columbia: Structural ore controls in the Cariboo (093A/H), Cassiar (104P) and Sheep Creek (082F) mining districts. Geoscience BC Report 2017-15, 108 p.

Andersen, T., 2002. Correction of common lead in U-Pb analyses that do not report 204Pb. Chemical Geology, vol. 192, p. 59–79.

Arne, D., Bierlin, F., Morgan, J. and Stein, H. 2001. Re-Os dating of sulfides associated with gold mineralization in central Victoria, Australia. Economic Geology, vol. 96, no. 6, p. 1455–1459.

Ayers, J., Dunkle, S., Gao, S. and Miller, C., 2002. Constraints on timing of peak and retrograde metamorphism in the Dabie Shan Ultrahigh-Pressure Metamorphic Belt, east-central China, using U-Th-Pb dating of zircon and monazite. Chemical Geology, vol. 186, p. 315–331.

Bailey, L.A., 2013. Late Jurassic fault-hosted gold mineralization of the Golden Saddle deposit, White Gold district, Yukon Territory. MSc thesis, University of British Columbia, Vancouver, BC, Canada, 170 p.

Berman, R.G., Ryan, J.J., Gordey, S.P. and Villeneuve, M., 2007. Permian to Cretaceous polymetamorphic evolution of the Stewart River region, Yukon-Tanana terrane, Yukon, Canada: P-T evolution linked with in-situ SHRIMP monazite geochronology. Journal of Metamorphic Geology, vol. 25, no. 7, p. 803–827.

Bierlein, F.P., Arne, D.C., Foster, D.A. and Reynolds, P., 2001. A geochronological framework for orogenic gold mineralisation in central Victoria, Australia. Mineralium Deposita, vol. 36, no. 8, p. 741–767.

Bierlein, F.P. and Crowe, D.E., 2000. Phanerozoic orogenic lode gold deposits. SEG Reviews, vol. 13, p. 103–139.

Bollinger, L. and Janots, E., 2006. Evidence for Mio-Pliocene retrograde monazite in the Lesser Himalaya, far western Nepal. European Journal of Mineralogy, vol. 18, no. 3, p. 289–297.

Brown, S., Fletcher, I., Stein, H., Snee, L. and Groves, D.I., 2002. Geochronological constraints on pre-, syn-, and postmineralization events at the world-class Cleo gold deposit, eastern goldfields province, Western Australia. Economic Geology, vol. 97, p. 541–559.

Breitsprecher, K. and Mortensen, J., 2004. YukonAge 2004: A database of isotopic age determinations for rock units from Yukon Territory. Yukon Geological Survey (CD-ROM).

Burke, M., Hart, C.J.R. and Lewis, L.L., 2005. Models for epigenetic gold exploration in the northern Cordilleran orogen, Yukon, Canada. *In:* Mineral deposit research: Meeting the global challenge, J. Mao and F.P. Bierlein (eds.), Proceedings of the Eighth Biennial SGA Meeting, Beijing, China, p. 525–528.

Catlos, E.J., 2013. Review: Versatile monazite: resolving geological records and solving challenges in materials science. Generalizations about monazite: Implications for geochronologic studies. American Mineralogist, vol. 98, no. 5–6, p. 819–832, doi:10.2138/am.2013.4336.

Chapman, R.J., Mortensen, J.K., Crawford, E.C. and LeBarge, W.P., 2010a. Microchemical studies of placer and lode gold in the Klondike district, Yukon, Canada: 1. Evidence for a small, gold-rich, orogenic hydrothermal system in the Bonanza and Eldorado Creek area. Economic Geology, vol. 105, no. 8, p. 1369–1392.

Chapman, R.J., Mortensen, J.K., Crawford, E.C. and Lebarge, W.P., 2010b. Microchemical studies of placer and Lode Gold in the Klondike district, Yukon, Canada: 2. Constraints on the nature and location of regional lode sources. Economic Geology, vol. 105, no. 8, p. 1393–1410.

Chapman, R.J., Mortensen, J.K. and LeBarge, W.P., 2011. Styles of lode gold mineralization contributing to the placers of the Indian River and Black Hills Creek, Yukon Territory, Canada as deduced from microchemical characterization of placer gold grains. Mineralium Deposita, vol. 46, no. 8, p. 881–903.

Cherniak, D.J., Watson, E.B., Grove, M. and Harrison, T.M., 2004. Pb diffusion in monazite: a combined RBS/SIMS study. Geochimica et Cosmochimica Acta, vol. 68, no. 4, p. 829–840.

Colpron, M., Nelson, J.L. and Murphy, D.C., 2006. A tectonostratigraphic framework for the pericratonic terranes of the northern Canadian Cordillera. Paleozoic Evolution and Metallogeny of Pericratonic Terranes at the Ancient Pacific Margin of North America, Canadian and Alaskan Cordillera, M. Colpron and J.L. Nelson (eds.), Geological Association of Canada, Special Paper, vol. 45, p. 1–23.

Colpron, M., McClelland, W.C., Piercey, S.J., Kroeger, E.D.L., Crowley, J.L. and Gehrels, G.E., 2025. Revisiting the “Klondike Orogeny”: Permian to Jurassic development of the Yukon-Tanana terrane, northern Canadian Cordillera. Tectonics, vol. 44, no. 6, e2024TC008748, doi:10.1029/2024TC008748.

Crawford, E.C., 2007. Klondike placer gold: New tools for examining morphology, composition and crystallinity. MSc thesis, University of British Columbia, Vancouver, BC, Canada, 151 p.

Crawford, E.C., Chapman, R.J., LeBarge, W.P. and Mortensen, J.K., 2007. Developing a new method to identify previously unrecognized geochemical and morphological complexity in placer gold deposits in western Yukon. In: Yukon Exploration and Geology 2006, D.S. Emond, L. Lewis and L.H. Weston (eds.), Yukon Geological Survey, p. 139–148.

Cuney, M. and Kyser, K., 2015. The geology and geochemistry of uranium and thorium deposits. Mineralogical Association of Canada Short Course Series, vol. 46, 362 p.

Didier, A., 2013. Compartment geochimique du chronometre U-Th-Pb dans la monazite: approche par analyses in-situ au LA-ICP_MS. PhD thesis, University Blaise Pascal, Clermont-Ferrand, France, 346 p.

Finger, F. and Krenn, E., 2007. Three metamorphic monazite generations in a high-pressure rock from the Bohemian Massif and the potentially important role of apatite in stimulating polyphase monazite growth along a PT loop. Lithos, vol. 95, no. 1-2, p. 103–115.

Frimmel, H.E., 2008. Earth's continental crustal gold endowment. Earth and Planetary Science Letters, vol. 267, no. 1-2, p. 45–55.

Gaidies, F., Morneau, Y.E., Petts, D.C., Jackson, S.E., Zagorevski, A. and Ryan, J.J., 2021. Major and trace element mapping of garnet: Unravelling the conditions, timing and rates of metamorphism of the Snowcap assemblage, west-central Yukon. Journal of Metamorphic Geology, vol. 39, no. 2, p. 133–164.

Gasquet, D., Bertrand, J.M., Paquette, J.L., Lehmann, J., Ratzov, G., De Ascencao Guedes, R., Tiepolo, M., Boullier, A.M., Scaillet, S. and Nomade, S., 2010. Miocene to Messinian deformation and hydrothermal activity in a pre-Alpine basement massif of the French western Alps: new U-Th-Pb and argon ages from the Lauziere massif. Bulletin de la Societe Geologique de France, vol. 181, p. 227–241.

Goldfarb, R.J., Baker, T., Dube, B., Groves, D.I., Hart, C.J.R. and Gosselin, P., 2005. Distribution, character, and genesis of gold deposits in metamorphic terranes. Economic Geology 100th Anniversary Volume, p. 407–450.

Goldfarb, R.J. and Groves, D.I., 2015. Orogenic gold: Common or evolving fluid and metal sources through time. Lithos, vol. 233, p. 2–26.

Goldfarb, R.J., Groves, D.I. and Gardoll, S., 2001. Orogenic gold and geologic time: a global synthesis. Ore Geology Reviews, vol. 18, p. 1–75.

Goldfarb, R.J., Newberry, R., Pickthorn, W. and Gent, C., 1991. Oxygen, hydrogen, and sulfur isotope studies in the Juneau gold belt, southeastern Alaska: Constraints on the origin of hydrothermal fluids. Economic Geology, vol. 86, p. 66–80.

Goldfarb, R.J. and Pitcairn, I., 2022. Orogenic gold: is a genetic association with magmatism realistic? Mineralium Deposita, vol. 58, p. 5–35.

Gordey, S.P. and Ryan, J. 2005. Geology, Stewart River Area (115N, 115-O and part of 115-J), Yukon Territory. Geological Survey of Canada, Open File 4970, scale 1:250 000.

Grand'Homme, A., 2016. Hydrothermal monazite: the unavoidable accessory. PhD thesis, Université Grenoble Alpes, Grenoble, France, 253 p.

Grand'Homme, A., Janots, E., Bosse, V., Seydoux-Guillaume, A.M. and De Ascencao Guedes, R., 2016. Interpretation of U-Th-Pb in-situ ages of hydrothermal monazite-(Ce) and xenotime-(Y): evidence from a large-scale regional study in clefts from the western Alps. Mineralogy and Petrology, vol. 110, no. 6, p. 787–807.

Grimshaw, M.R., 2018. Gold Mineralisation in the Lone Star area of the Klondike Gold District, Yukon, Canada. PhD thesis, University of Leeds, Leeds, England, 354 p.

Groves, D.I., Goldfarb, R.J., Gebre-Mariam, M., Hagemann, S.G. and Robert, F., 1998. Orogenic gold deposits: A proposed classification in the context of their crustal distribution and relationship to other gold deposit types. Ore Geology Reviews, vol. 13, p. 7–27.

Groves, D.I., Goldfarb, R.J., Robert, F. and Hart, C.J.R., 2003. Gold deposits in metamorphic belts: overview of current understanding, outstanding problems, future research, and exploration significance. Economic Geology, vol. 98, p. 1–29.

Henley, R., Norris, R. and Paterson, C., 1976. Multistage ore genesis in the New Zealand geosyncline: A history of post-metamorphic lode emplacement. Mineralium Deposita, vol. 11, p. 180–196.

Hilgers, C., Koehn, D., Bons, P.D. and Urai, J., 2001. Development of crystal morphology during unitaxial growth in a progressively widening vein: II. Numerical simulations of the evolution of antitaxial fibrous veins. Journal of Structural Geology, vol. 23, p. 873–885.

Horstwood, M.S.A., Foster, G.L., Parrish, R.R., Noble, S.R. and Nowell, G.M., 2003. Common-Pb corrected in situ U–Pb accessory mineral geochronology by LA-MC-ICP-MS. Journal of Analytical Atomic Spectrometry, vol. 18, no. 8, p. 837–846.

Hoymann, K.H. and Friedrich, G., 1990. Gold and sulphide mineralization in the Hunker Creek area, Yukon Territory, Canada. Yukon Geology, vol. 3, p. 312–326.

Hunt, P.A. and Roddick, J.C., 1992. A compilation of K-Ar ages, report 21. Geological Survey of Canada, Radiogenic age and isotopic studies, Report 5, Paper 91-2, p. 207–252.

Jochum, K., Willbold, M., Raczek, I., Stoll, B. and Herwig, K., 2005. Chemical Characterisation of the USGS Reference Glasses GSA-1G, GSC-1G, GSD-1G, GSE-1G, BCR-2G, BHVO-2G, and BIR-1G Using EPMA, ID-TIMS, ID-ICP-MS, and LA-ICP-MS. Geostandards and Geoanalytical Research, vol. 29, no. 3, p. 285–302.

Johnson, T.E., Clark, C., Taylor, R.J.M., Santosh, M. and Collins, A.S., 2015. Prograde and retrograde growth of monazite in migmatites: An example from the Nagercoil Block, southern India. Geoscience Frontiers, vol. 6, no. 3, p. 373–387.

Joyce, N.L., Ryan, J.J., Colpron, M., Hart, C.J.R. and Murphy, D.C., 2015. A compilation of $^{40}Ar/^{39}Ar$ age determinations for igneous and metamorphic rocks, and mineral occurrences from central and southeast Yukon. Geological Survey of Canada, Open File 7924, 229 p.

Jutras, M. and Kenwood, S., 2022. NI 43-101 technical report on the Klondike district gold project, Yukon Territory, Canada. Prepared for Klondike Gold Corp., issued December 16, 2022, 315 p.

Kerrich, R. and King, R., 1993. Hydrothermal zircon and baddeleyite in Val d'Or Archaean mesothermal gold deposits: characteristics, composition and fluid inclusion properties with implication for timing of primary gold mineralization. Canadian Journal of Earth Sciences, vol. 30, p. 2334–2351.

Knight, J.B., Morison, S.R. and Mortensen, J., 1999a. The relationship between placer gold particle shape, rimming and distance of fluvial transport; as exemplified by gold from the Klondike district, Yukon Territory, Canada. Economic Geology, vol. 94, p. 635–648.

Knight, J.B., Mortensen, J.K. and Morison, S.R., 1999b. Lode and placer gold composition in the Klondike district, Yukon Territory, Canada: Implications for the nature and genesis of Klondike placer and lode gold deposits. Economic Geology, vol. 94, p. 649–664.

Kohn, M.J. and Malloy, M.A., 2004. Formation of monazite via prograde metamorphic reactions among common silicates: implications for age determinations. Geochimica et Cosmochimica Acta, vol. 68, p. 101–113, doi:10.1016/S0016-7037(03)00258-8.

Kretz, R., 1983. Symbols for rock-forming minerals. American Mineralogist, vol. 68, p. 277–279.

Kylander-Clark, A.R.C., Hacker, B.R. and Cottle, J.M., 2013. Laser-ablation split-stream ICP petrochronology. Chemical Geology, vol. 345, p. 99–112.

Lin, S. and Corfu, F., 2002. Structural setting and geochronology of auriferous quartz veins at the High Rock Island gold deposit, northwestern Superior Province, Manitoba, Canada. Economic Geology, vol. 97, p. 43–57.

MacKenzie, D.J., Craw, D. and Mortensen, J.K., 2008a. Structural controls on orogenic gold mineralisation in the Klondike goldfield, Canada. Mineralium Deposita, vol. 43., no. 4, p. 435–448.

MacKenzie, D., Craw, D., Mortensen, J.K. and Liverton, T., 2008b. Disseminated gold mineralization associated with orogenic veins in the Klondike Schist, Yukon. *In:* Yukon Exploration and Geology 2007, D.S. Emond, L.R. Blackburn, R.P. Hill and L.H. Weston (eds.), Yukon Geological Survey, p. 215–224.

Mortensen, J.K., 1990. Geology and U–Pb geochronology of the Klondike district, west-central Yukon Territory. Canadian Journal of Earth Sciences, vol. 27, no. 7, p. 903–914.

Mortensen, J.K., 1996. Geological compilation maps of the northern Stewart River map area, Klondike and Sixtymile Districts (115N/15, 16; 1150/13, 14; and parts of 1150/15, 16). Exploration and Geological Services Division, Yukon Region, Indian and Northern Affairs Canada, Open File 1996-1(G), six 1:50 000-scale maps.

Mortensen, J.K., Chapman, R., LeBarge, W. and Jackson, L., 2004. Application of placer and lode gold geochemistry to gold exploration in western Yukon. *In:* Yukon Exploration and Geology 2004, D.S. Emond, L.L. Lewis and G.D. Bradshaw (eds.), Yukon Geological Survey, p. 205–212.

Mortensen, J.K., Chapman, R.J., LeBarge, W. and Crawford, E.C., 2006. Compositional studies of placer and lode gold from western Yukon: Implications for lode sources. *In:* Yukon Exploration and Geology 2005, D.S. Emond, G.D. Bradshaw, L.L. Lewis and L.H. Weston (eds.), Yukon Geological Survey, p. 247–255.

Mortensen, J.K., Craw, D., MacKenzie, D.J., Gabites, J.E. and Ullrich, T., 2010. Age and origin of orogenic gold mineralization in the Otago Schist Belt, South Island, New Zealand: constraints from lead isotope and 40Ar/39Ar dating studies. Economic Geology, vol. 105, no. 4, p. 777–793.

Mortensen, J.K., Liverton, T. and Dodd, K., 2019. Chemostratigraphic constraints on the nature and origin of felsic schist units hosting stratabound and orogenic vein gold on Lone Star ridge, Klondike gold district, Yukon. Journal of Geochemical Exploration, vol. 204, p. 112–130.

Mortensen, J.K., Nesbitt, B.E. and Rushton, R.W., 1992. Preliminary observations on the geology and geochemistry of quartz veins in the Klondike district, West-Central Yukon. Yukon Geology, vol. 3, p. 260–270.

Mortensen, J.K., Rhys, D.A. and Ross, K.V., 2011. Investigations of orogenic gold deposits in the Cariboo gold district, east-central British Columbia: final report. Summary of Activities 2010, Geoscience BC, Report 2011-1, p. 65–76.

Mortensen, J.K., Craw, D. and MacKenzie, D.J., 2023. Concepts and revised models for Phanerozoic orogenic gold deposits. *In:* Recent Advances in Understanding Gold Deposits: from Orogeny to Alluvium, T. Torvela, J.S. Lambert-Smith and R.J. Chapman (eds.), Geological Society of London Special Publication, vol. 516, p. 15–46, doi:10.1144/SP516-2021-39.

Nelson, J.L., Colpron, M. and Israel, S., 2013. The Cordillera of British Columbia, Yukon, and Alaska: Tectonics and metallogeny. *In:* Metallogeny and Discovery: The North American Cordillera and Similar Accretionary Settings, M. Colpron, T. Bissig, B.G. Rusk and J.F.H. Thompson (eds.), Society of Economic Geologists Special Publication, vol. 17, p. 53–109.

Overstreet, W., 1967. The geologic occurrence of monazite. United States Geological Survey Professional Paper, vol. 530, p. 327.

Paquette, J.-L., N´ed´elec, A., Moine, B. and Rakotondrazafy, M., 1994. U-Pb, single zircon Pb-evaporation, and Sm-Nd isotopic study of a granulite domain in SE Madagascar. The Journal of Geology, vol. 102, no. 5, p. 523–538.

Paquette, J.L. and Tiepolo, M., 2007. High resolution (5 micron) U-Th-Pb isotope dating of monazite with excimer laser ablation (ELA)-ICPMS. Chemical Geology, vol. 240, no. 3-4, p. 222–237.

Pearce, J.A., 1996. A user's guide to basalt discrimination diagrams. In: Trace element geochemistry of volcanic rocks: applications for massive sulphide exploration, Wyman, D. A. (eds.), Geological Association of Canada, short course notes, v. 12, p. 79–113.

Petrus, J.A. and Kamber, B.S., 2012. VizualAge: A novel approach to Laser Ablation ICP-MS U-Pb geochronology data reduction. Geostandards and Geoanalytical Research, vol. 36, no. 3, p. 247–270.

Pitcairn, I., Teagle, D., Craw, D., Olivo, G., Kerrich, R. and Brewer, T., 2006. Sources of metals and fluids in orogenic gold deposits: Insights from the Otago and Alpine schists, New Zealand. Economic Geology, vol. 101, p. 1525–1546.

Pyle, J.M. and Spear, F.S., 1999. Yttrium zoning in garnet: Coupling of major and accessory phases during metamorphic reactions. Geological Materials Research, vol. 1, no. 6, p. 1–49.

Rasmussen, B., Fletcher, I.R. and Muhling, J.R., 2007. In situ U–Pb dating and element mapping of three generations of monazite: Unravelling cryptic tectonothermal events in low-grade terranes. Geochimica et Cosmochimica Acta, vol. 71, no. 3, p. 670–690.

Rasmussen, B., Sheppard, S. and Fletcher, I.R., 2006. Testing ore deposit models using in situ U-Pb geochronology of hydrothermal monazite: Paleoproterozoic gold mineralization in northern Australia. Geology, vol. 34, no. 2, p. 77–80.

Reiners, P.W. and Brandon, M.T., 2006. Using thermochronology to understand orogenic erosion. Annual Review of Earth and Planetary Sciences, vol. 34, no. 1, p. 419–466.

Rhys, D.A., Mortensen, J. and Ross, K.V., 2009. Investigations of orogenic gold deposits in the Cariboo gold district, east-central British Columbia (Parts of NTS 093A, H): Progress Report. Geoscience BC Summary of Activities 2008, Geoscience BC, Report 2009-1, p. 49–74.

Rushton, R.W., Nesbitt, B.E., Muehlenbachs, K. and Mortensen, J.K., 1993. A fluid inclusion and stable isotope study of Au quartz veins in the Klondike district, Yukon Territory, Canada: A section through a mesothermal vein system. Economic Geology, vol. 88, no. 3, p. 647–678.

Rusk, B., 2012. Cathodoluminescent Textures and Trace Elements in Hydrothermal Quartz. *In:* Quartz: Deposits, Mineralogy and Analytics, J. Götze and R. Möckel (eds.), Springer Geology, Springer, Berlin, Heidelberg, p. 307–329, https://doi.org/10.1007/978-3-642-22161-3_14.

Salier, B., Groves, D.I., McNaughton, N.J. and Fletcher, I., 2005. Geochronological and stable isotope evidence for widespread orogenic gold mineralization from a deep-seated fluid source at ca 2.65 Ga in Laverton gold province, Western Australia. Economic Geology, vol. 100, p. 1363–1388.

Sarma, D.S., McNaughton, N.J., Fletcher, I., Groves, D.I., Mohan, M.R. and Balaram, V., 2008. Timing of gold mineralization in the Hutti gold deposit, Dharwar Craton, South India. Economic Geology, vol. 103, p. 1715–1727.

Schandl, E.S. and Gorton, M.P., 2004. A textural and geochemical guide to the identification of hydrothermal monazite: Criteria for selection of samples for dating epigenetic hydrothermal ore deposits. Economic Geology, vol. 99, p. 1027–1035.

Scharer, U., 1984. The effect of initial ^{230}Th disequilibrium on young U-Pb ages: the Makalu case, Himalaya. Earth and Planetary Science Letters, vol. 67, p. 191–204.

Selby, D., Creaser, R.A., Hart, C.J.R., Romback, C.S., Thompson, J.F.H., Smith, M.T., Bakke, A.A. and Goldfarb, R.J., 2002. Absolute timing of sulfide and gold mineralization: A comparison of Re-Os molybdenite and Ar-Ar mica methods from the Tintina gold belt, Alaska. Geology, vol. 30, no. 9, p. 791–794.

Seydoux-Guillaume, A.-M., Paquette, J.-L., Wiedenbeck, M., Montel, J.-M. and Heinrich, W., 2002a. Experimental resetting of the U–Th–Pb systems in monazite. Chemical geology, vol. 191, no. 1, p. 165–181.

Seydoux-Guillaume, A.-M., Wirth, R., Nasdala, L., Gottschalk, M., Montel, J.M. and Heinrich, W., 2002b. An XRD, TEM and Raman study of experimentally annealed natural monazite. Physics and Chemistry of Minerals, vol. 29, no. 4, p. 240–253.

Spear, F.S. and Pyle, J.M., 2002. Apatite, monazite, and xenotime in metamorphic rocks. Reviews in Mineralogy and Geochemistry, vol. 48, no. 1, p. 293–335.

Staples, R.D., 2014. Diachronous Deformation, Metamorphism and Exhumation in the Northern Canadian Cordillera: Revealed from Pressure-Temperature-Time-Deformation Paths of Former Mid-Crustal Rocks. PhD thesis, Simon Fraser University, Vancouver, BC, Canada, 243 p.

Staples, R.D., Gibson, H.D., Berman, R.G., Ryan, J.J. and Colpron, M., 2013. A window into the Early to mid-Cretaceous infrastructure of the Yukon-Tanana terrane recorded in multi-stage garnet of west-central Yukon, Canada. Journal of Metamorphic Geology, vol. 31, no. 7, p. 729–753.

Staples, R.D., Gibson, H.D., Colpron, M. and Ryan, J.J., 2016. An orogenic wedge model for diachronous deformation, metamorphism, and exhumation in the hinterland of the northern Canadian Cordillera. Lithosphere, vol. 8, no. 2, p. 165–184.

Stroh, B., 2019. Resolving Monazite Growth Mechanisms in Orogenic Gold Settings: A Study from the Klondike Gold District, Western Yukon. MSc thesis, University of British Columbia, Vancouver, BC, Canada, 451 p.

Stuwe, K., 1998. Tectonic constraints on the timing relationships of metamorphism, fluid production and gold-bearing quartz vein emplacement. Ore Geology Reviews, vol. 13, p. 219–228.

Taylor, R.D., Goldfarb, R.J., Monecke, T., Fletcher, I.R., Cosca, M.A. and Kelly, N.M., 2015. Application of U-Th-Pb phosphate geochronology to young orogenic gold deposits: New age constraints on the formation of the Grass Valley gold district, Sierra Nevada foothills province, California. Economic Geology, vol. 110, no. 5, p. 1313–1337.

Tera, F. and Wasserburg, G.J., 1972. U-Th-Pb systematics in three apollo 14 basalts and the problem of initial Pb in lunar rocks. Earth and Planetary Science Letters, vol. 14, p. 281–304.

Van Emden, B., Thornber, M., Graham, J. and Lincoln, F., 1997. The incorporation of actinides in monazite and xenotime from placer deposits in Western Australia. The Canadian Mineralogist, vol. 35, p. 95–104.

Vielreicher, N.M., Groves, D.I., Fletcher, I.R., McNaughton, N.J. and Rasmussen, B., 2003. Hydrothermal monazite and xenotime geochronology: A new direction for precise dating of orogenic gold mineralization. Society of Economic Geologists Newsletter, vol. 53, p. 1–16.

Vry, J., Powell, R., Golden, K.M. and Petersen, K., 2010. The role of exhumation in metamorphic dehydration and fluid production. Nature Geoscience, vol. 3, no. 1, p. 31–35.

Wetherill, G.W., 1956. Discordant uranium-lead ages, I. Transactions, American Geophysical Union, vol. 37, no. 3, p. 320–326.

White, A.J.R., Waters, D.J. and Robb, L.J., 2015. Exhumation-driven devolatilization as a fluid source for orogenic gold mineralization at the Damang deposit, Ghana. Economic Geology, vol. 110, no. 4, p. 1009–1025.

Williams, M.L., Jercinovic, M.J., Harlov, D.E., Budzyń, B. and Hetherington, C.J., 2011. Resetting monazite ages during fluid-related alteration. Chemical Geology, vol. 283, no. 3-4, p. 218–225.

Williams, M.L., Jercinovic, M.J. and Hetherington, C.J., 2007. Microprobe monazite geochronology: Understanding geologic processes by integrating composition and chronology. Annual Review of Earth and Planetary Sciences, vol. 35, no. 1, p. 137–175.

Winchester, J. and Floyd, P., 1977. Geochemical discrimination of different magma series and their differentiation products using immobile elements. Chemical Geology, vol. 20, p. 325–343.

Wolff, W.R.G., 2012. Microstructures and Trace Element Signatures of Orogenic Quartz Veins in the Klondike District, Yukon Territory, Canada. BSc thesis, University of British Columbia, Vancouver, BC, Canada, 76 p.

Yukon Geological Survey, 2010. Yukon MINFILE - A database of mineral occurrences. Yukon Geological Survey, https://data.geology.gov.yk.ca/Occurrences/ [accessed 24/05/2017].

Yukon Geolocial Survey, 2023. Yukon Geochronology – A database of Yukon isotopic age determinations. Yukon Geological Survey, https://data.geology.gov.yk.ca/Compilation/22 [accessed 18/09/2025].

Zhu, X.K. and O'Nions, E.K., 1999. Zonation of monazite in metamorphic rocks and its implications for high temperature thermochronology: A case study from the Lewisian terrain. Earth and Planetary Science Letters, vol. 171, p. 209–220.